CSIRO
AUSTRALIA

A Soil-Canopy Scheme for Use in a Numerical Model of the Atmosphere - 1D Stand-Alone Model.

E.A. Kowalczyk, J.R. Garratt and P.B. Krummel

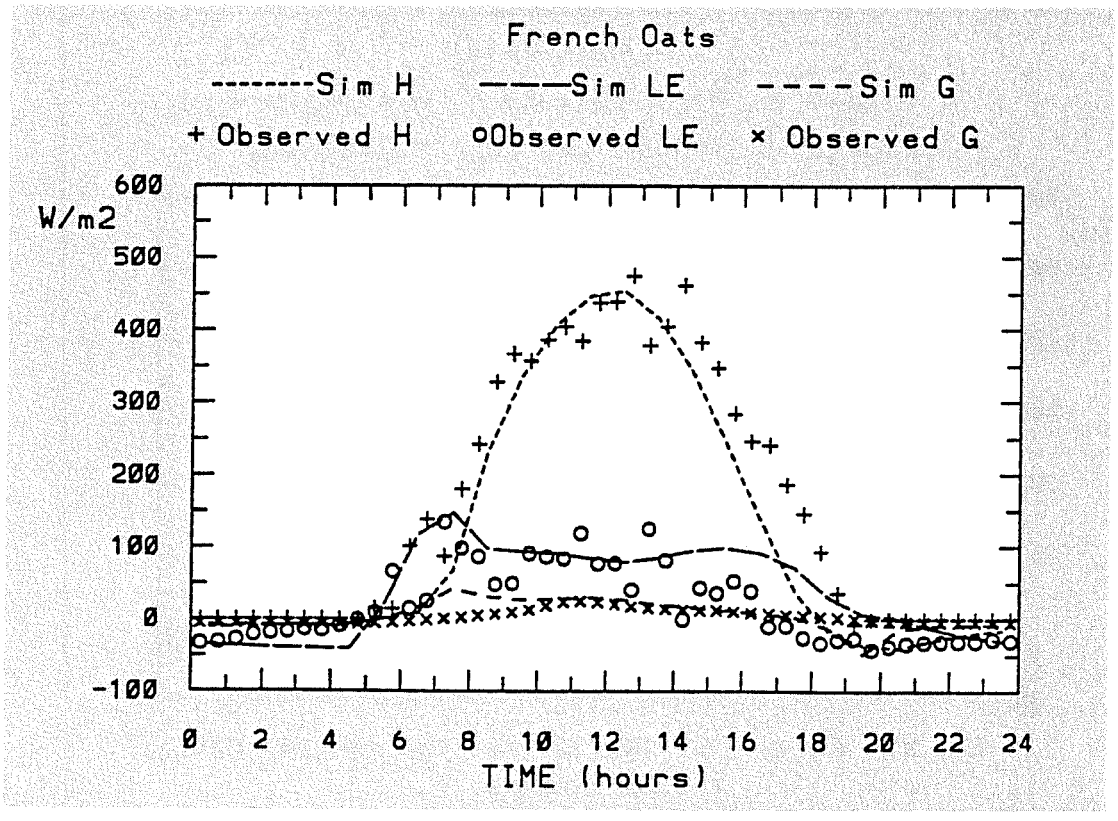

CSIRO DIVISION OF ATMOSPHERIC RESEARCH
TECHNICAL PAPER NO.23

CSIRO
AUSTRALIA

A Soil-Canopy Scheme for Use in a Numerical Model of the Atmosphere - 1D Stand-Alone Model.

E.A. Kowalczyk, J.R. Garratt and P.B. Krummel

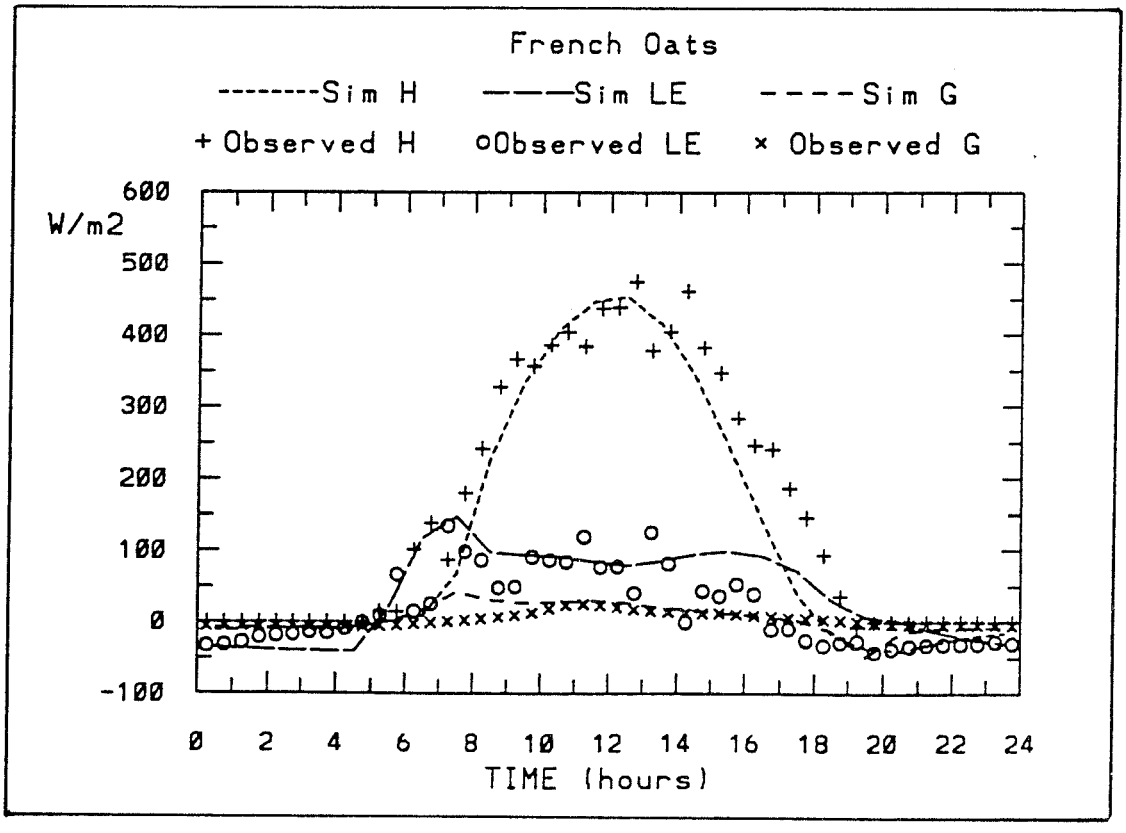

CSIRO DIVISION OF ATMOSPHERIC RESEARCH
TECHNICAL PAPER NO.23

National Library of Australia Cataloguing-in-Publication Entry

Kowalczyk, E. A. (Eva A.).
A soil-canopy scheme for use in a numerical model of the atmosphere - 1D stand-alone model.
Bibliography ISBN 0 643 05248 8
1. Soil-canopy temperature - Mathematical models
2. Soil moisture - Mathematical models
3. Atmospheric circulation - Mathematical models
I. Garratt, J.R. (John R.). II. Krummel, P.B. (Paul B.). III. CSIRO Division of Atmospheric Research. IV. Title. (Series: Division of Atmoshperic Research. Technical Paper; no. 23).
631.43

A Soil-Canopy Scheme for Use in a Numerical Model of the Atmosphere - 1D Stand-Alone Model.

E.A. Kowalczyk, J.R. Garratt and P.B. Krummel
CSIRO, Division of Atmospheric Research Private Bag 1, Mordialloc,
Vic 3195, Australia

Abstract

We provide a detailed description of a soil-canopy scheme for use in the CSIRO GCMs (CSIRO-4 and CSIRO-9), in the form of a one-dimensional stand-alone model. In addition, the paper documents the model's ability to simulate realistic surface fluxes by comparison with mesoscale model simulations (involving more sophisticated soil and boundary-layer treatments) and observations, and the diurnal range in surface quantities, including extreme maximum surface temperatures. The sensitivity of the model to values of the surface resistance is also quantified.

The model represents phase 1 of a longer-term plan to improve the ABL and surface schemes in the CSIRO GCMs.

1 Introduction

The main purpose of any parameterization of the land surface and the atmospheric boundary layer (ABL) for use in general circulation models (GCM) is to provide an efficient means of calculating the fluxes of momentum, heat and water vapour, both at the surface and at several levels within the ABL. The surface parameterization should include the effects of surface albedo (radiative transfer), surface roughness (momentum transfer), and surface hydrology (sensible and latent heat transfer). All of these properties are influenced by the presence of vegetation.

The inclusion of realistic soil and vegetation schemes in numerical dynamical models has taken on added importance in recent times because of the increased interest in land-use activities, and their impact on climate. The rapidly growing interest in climate and climate change problems, and the need to simulate regional climate more precisely on time scales of several decades, is leading to a greater appreciation of the role of the ABL and of the land surface in the climate system. It is generally accepted that in short-range numerical weather prediction models, the initialization problem and initial data deficiencies are far more crucial than details of the model physics. In contrast, there is a recognition that climate is sensitive to the characteristics of the underlying surface (in particular, the albedo and moisture availability), and that the accuracy of the surface-flux formulation becomes more important for longer-range forecasts and for climate simulations.

In recent years, quite sophisticated turbulence, soil and canopy schemes have been formulated for use in GCMs, and at the same time very detailed data sets have become available for specifying the geographical distribution of a range of surface parameters (see e.g. Dorman and Sellers, 1989). Carson (1982) has given a comprehensive review of land-surface and ABL schemes used in many GCMs up to c. 1980, with an emphasis on surface processes. References to other papers which complement this earlier review, and tend to discuss specific topics in more detail, can be found in Garratt (1992a).

The four land-surface properties - albedo, roughness, hydrology (degree of wetness) and vegetation density - have all been the subject of individual sensitivity studies. In the real world, each of these properties varies significantly in space and time though it is not yet clear to what extent GCMs need to incorporate these natural variations. As an example, the albedo over snow-free land is known to vary between about 10 percent for tropical forest and 35 percent for desert (see Fig.1). Likewise, the surface roughness over flat terrain can vary between 1 mm or less over sand and snow to 1-2 m over tall forests (see Fig.2). These roughness values are likely to be higher in the presence of small-scale orographic features.

Data sets may be required for three main purposes - specification of the lower boundary conditions, specification of initial conditions and for comparison with model output. In the first case, we are looking at data sets which allow the soil/vegetation type, the albedo, the aerodynamic roughness and the mean height of the orography to be specified as a function of geographical location. In the second case, climatological variables may be

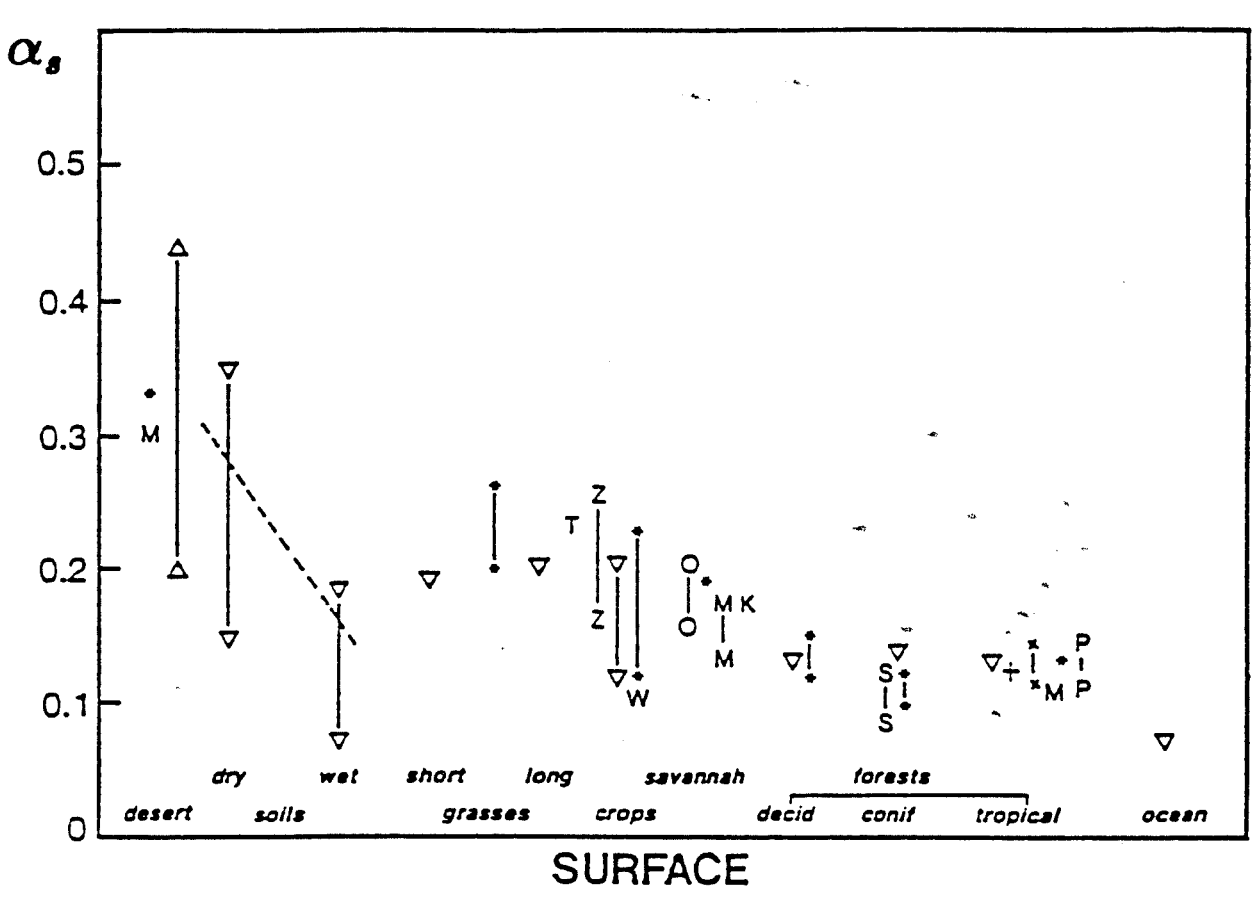

Figure 1: Variation of albedo with surface type, based on observations, literature values and model-specified values. Data for both wet and dry soils, short and long grasses and deciduous, coniferous and tropical forests are shown. Vertical bars represent the range of albedo values for the specific surface type, whilst the dashed line represents the dependence of albedo upon surface moisture content given by Idso et al. (1975), viz.

$$\alpha_s = \begin{cases} 0.31 - 0.34\eta_g/\eta_{sat} & \eta_g/\eta_{sat} \leq 0.5 \\ 0.14 & \eta_g/\eta_{sat} \geq 0.5. \end{cases}$$

Data represent both direct observations and model-assumed values (themselves based on observations), with symbols as follows: (*) from Dorman and Sellers (1989), including a range of values for wheat (W); (∇) from Wilson and Henderson-Sellers (1985), their Tables 8 and 9 - the ocean value is for a high zenith angle; ($\triangle$) from Henderson-Sellers and Wilson (1983), their Table 4; (Z) from Sellers et al. (1986) for a wheat crop, giving the variation in albedo with zenith angle; (M) from Matthews (1985); ($\bigcirc$) from Oguntoyinbo (1970); (T) from Tapper (1988); (K) from Kriebel (1979); (S) from Stewart (1971); (P) from Pinker et al. (1980); (x) from Dorman and Sellers (1989)(due to Monteny), see also Oguntoyinbo (1970); (+) from Shuttleworth et al. (1984a).

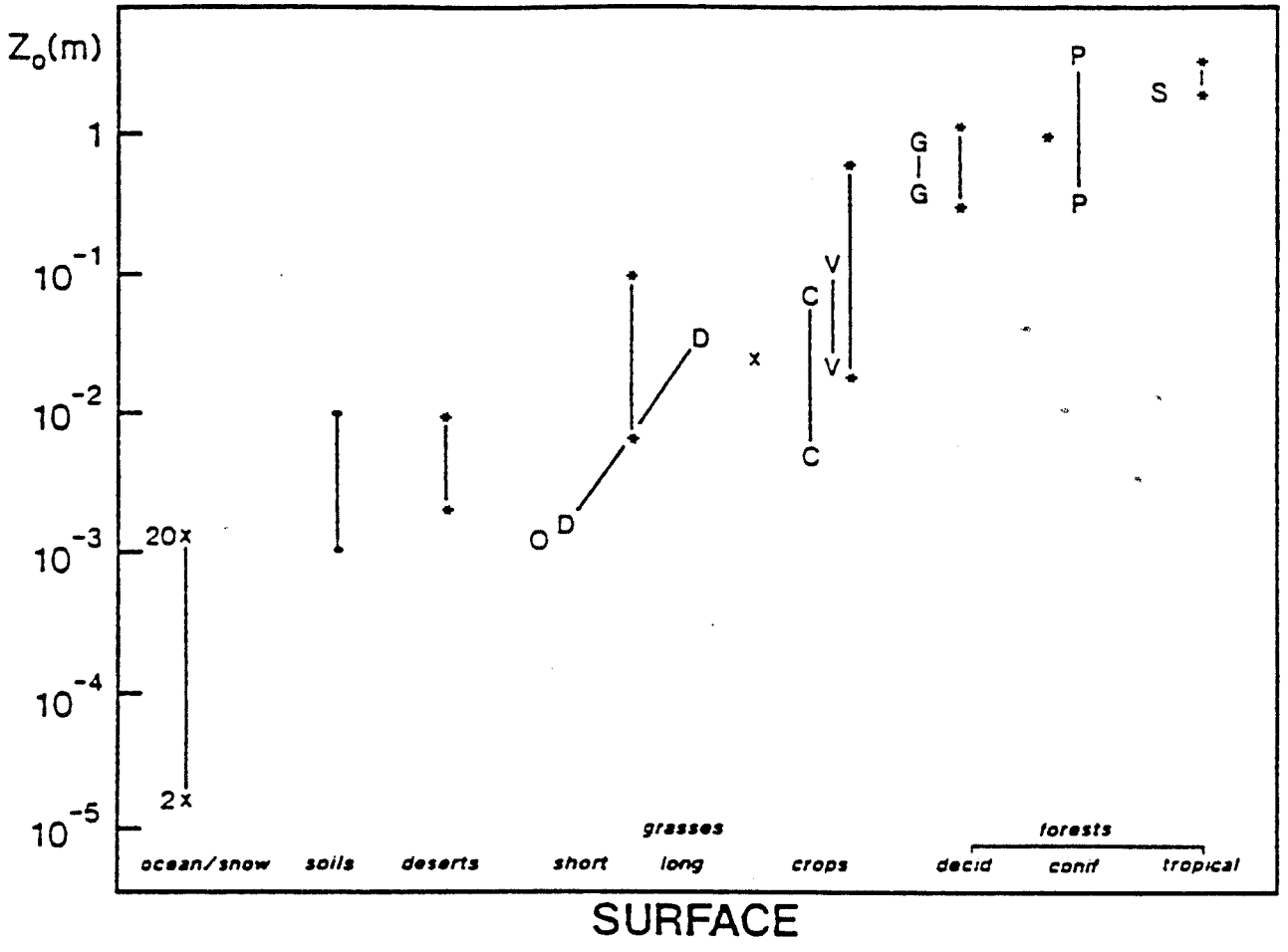

Figure 2: Variation of surface roughness length with surface type, based on observations, literature values and model-specified values. Symbols as follows: (*) from Dorman and Sellers (1989) for some of their 12 surface types; (x) from Garratt (1977) for the ocean (or blowing snow) for wind speeds (measured at 10m height) in the range 2 to 20 ms^{-1}; (x) from Izumi (1971) for a wheat stubble; (G) from Garratt (1980) for sub-tropical savannah; (C) from Clarke et al. (1971) for a semi-arid sparse grass cover; (V) from Hicks (1973) for a vineyard; (P) and (C) from Garratt (1991); (S) from Shuttleworth et al. (1984b) for a tropical rain forest; (D) from Deacon (1953), with the straight line representing the variation of z_0 with grass height.

available to initialise a model integration - these may be in the form of mean monthly atmospheric variables as a function of height and location, or of surface variables as a function of season and location. In general, accurate initialisation of a climate model is not a major requirement, in contrast to the needs of numerical weather prediction, but a realistic initialisation of the soil moisture field for example may be required. In the third case, validation of model simulations depends on the availability of observations, suitably reduced and averaged, for comparison with model output. Observations might take the form of time-averaged atmospheric fields of velocity, temperature and humidity, derived fields of stream function and velocity potential; surface fields of pressure, fluxes, precipitation; climatological fields of clouds, and detailed data on surface variables in terms of diurnal behaviour at specific locations. Perrier (1982) should be consulted for an earlier discussion on data sets useful for validation of models and suitable for specifying lower boundary conditions.

There are some 10 - 20 major GCMs in use around the world and, until the late 1980s, most had quite crude surface schemes. In recent times, a number of relatively sophisticated canopy schemes have become available for use in both mesoscale models and GCMs (e.g. BATS - Dickinson et al., 1986; SiB - Sellers et al., 1986; Noilhan and Planton, 1989). Such schemes owe much to the work of Deardorff (1978).

The main CSIRO GCMs at 31/12/91 included the 4-level model CSIRO4 (Hunt and Gordon, 1989) and its companion in the form of a 9-level version (CSIRO9). Both utilised the soil-moisture scheme of Deardorff (1977), with a single soil type only, constant roughness length over land and no allowance for vegetation. CSIRO4 used the forcing method (Deardorff, 1978) for calculation of surface temperature - this neglects the soil heat flux - and CSIRO9 uses the finite difference form of the thermal diffusion equation with three soil layers. The soil-canopy scheme described in this technical paper, and its incorporation into the low-resolution (rhomboidal 21) version of both CSIRO4 and CSIRO9 models, and the high-resolution (rhomboidal 42) version of the CSIRO4 model, represent Phase 1 of a long-term plan to improve the representation of ABL and surface processes in CSIRO GCMs. The scheme gives a significant improvement on earlier methods of surface representation in CSIRO models. At the same time, the data sets described in Dorman and Sellers (1989), with small local modifications, are being used to describe the geographical distribution of surface albedo, roughness and unconstrained canopy (stomatal) resistance. This requires averaging of the original $1^0 \times 1^0$ data for 12 surface types for compatibility with the hori-

zontal grid structure in both low (R21) and high (R42) resolution versions of CSIRO4 and CSIRO9. Phase 2 of the plan involves the assessment and ultimate incorporation into future model versions of detailed and comprehensive schemes for the surface and ABL.

The main purposes of the present technical paper are as follows -

(a) To provide a detailed description of the soil-canopy scheme to be used in CSIRO4 and CSIRO9.

(b) To demonstrate the realistic simulation of the diurnal variation of a number of quantities, by comparison with observations.

(c) To document the model's ability to simulate realistic surface fluxes.

(d) To document the diurnal range in surface quantities, including surface temperature.

(e) To quantify the sensitivity of the soil-canopy model to values of the roughness length and surface resistance.

The soil-canopy scheme described here has a number of features similar to those described in Deardorff (1978) and Noilhan and Planton (1989). It allows for the inclusion of the following details - soil type (hence variable thermal and moisture properties); albedo; roughness length; canopy resistance; canopy interception of moisture; runoff; deep-soil percolation; snow accumulation and melting.

2 Basic Formulations for Land-Surface Processes and the ABL used in GCMs.

(a) Surface fluxes

Surface fluxes (stress τ, sensible heat flux H and evaporation E) are related to mean properties of the flow through the use of drag and bulk transfer relations. These are written,

$$\tau/\rho = -\overline{u'w'} = u_*^2 = C_D u_a^2 \quad (1)$$

$$H/\rho c_p = \overline{w'\theta'} = -u_*\theta_* = C_H u_a(\theta_o - \theta_a) \quad (2)$$

$$E/\rho = \overline{w'q'} = -u_* q_* = C_E u_a (q_o - q_a) \quad (3)$$

$$E_p/\rho = C_E u_a (q_o^* - q_a), \quad (4)$$

where E_p is the value of evaporation E when the surface is saturated at temperature T_o. In the above, u_a, θ_a and q_a are model variables at level 1, and θ_o , q_o are surface values (θ_o is the potential temperature associated with the absolute radiative temperature T_o; also $q_o^* = q_o^*(T_o)$).

In these equations, formulation of the bulk transfer coefficients (C_D, C_H and C_E) depends on the reference level for the atmospheric variables u_a, θ_a and q_a. If the lowest model level lies within the surface layer, the formulation is based on Monin-Obukhov similarity theory, otherwise generalised boundary-layer similarity theory needs to be used, Garratt (1991). In both CSIRO GCMs, surface-layer theory is used - in CSIRO9, with the lowest level at about 150m, that based on Louis (1979). In CSIRO4, with the lowest level at about 900 mbar, an interpolation technique is used to give pseudo-variables at a nominal level of $100m$, and transfer coefficients evaluated from standard surface-layer theory.

The drag, heat and mass transfer coefficients discussed above take into account both turbulent and molecular transfer of a property s between the surface (property concentration s_o) and reference height z in the surface layer (concentration s). For some applications, it may be more convenient to replace the transfer coefficients by quasi-resistance parameters. The bulk aerodynamic resistance to the transfer of momentum from a level z to the surface, i.e. at $z = z_o$, is defined as

$$r_{aM} = \rho u_a(z)/\tau_o = u_a(z)/u_{*o}^2 = (C_D u_a)^{-1}. \quad (5)$$

and so as C_D increases (higher z_o or more unstable conditions) or u_a increases, the resistance decreases. For a reference height of $10m$, and with $u_a = 5ms^{-1}$, it is readily deduced that r_{aM} typically lies in the range $10 - 100sm^{-1}$ for land surfaces. Expressions for the bulk aerodynamic resistance to sensible and latent heat exchange can be defined as

$$r_{aH} = \rho c_p(\theta_o - \theta_a)/H_o = (\theta_a - \theta_o)/u_{*o}\theta_{*o} \quad (6)$$

$$r_{aV} = \rho(q_o - q_a)/E_o = (q_a - q_o)/u_{*o}q_{*o}. \quad (7)$$

Comparison with Eqs.2 and 3 gives,

$$r_{aH} = (C_H u_a)^{-1} \quad (8)$$

$$r_{aV} = (C_E u_a)^{-1}, \quad (9)$$

so that for land surfaces in particular, where $C_{H,E} < C_D$, it follows that $r_{aH} \approx r_{aV} > r_{aM}$. An alternative form of the bulk transfer relations, Eqs.2 and 3, is then

$$H_o/\rho c_p = (\theta_o - \theta_a)/r_{aH} \tag{10}$$

$$E_o/\rho = (q_o - q_a)/r_{aV}. \tag{11}$$

The potential evaporation (E) is written as,

$$E_p = \rho(q^*(T_o) - q_a)/r_{aV}. \tag{12}$$

In the calculation of evaporation, a general or effective surface resistance, r_s , can be used to take into account the effect of vegetation on evaporation. For a canopy, this resistance is almost entirely determined by the stomatal resistance of the leaves, and called a bulk stomatal resistance, given by

$$r_{st} = \rho(q^*(T_o) - q_o)/E_o. \tag{13}$$

This equation is commonly referred to as the 'big-leaf' model, since it basically represents the whole canopy as a single hypothetical 'leaf' of resistance r_{st} . Now if r_{sti} is the resistance of a single stomata, then r_{st} is defined as the parallel sum of these stomatal resistances, with

$$1/r_{st} = A^{-1} \sum_i L_{A,i}/r_{sti}, \tag{14}$$

where $L_{A,i}$ is the area of the ith leaf and the summation is over all leaves above some representative ground area A. The leaf area index (LAI) would be defined as the total leaf area of the foliage per unit ground area.

The surface resistance, r_s, will be similar to r_{st} for a complete canopy cover, but will be different from r_{st} for partial cover. The resistance r_s in the latter case would include effects of evaporation from the soil which contributes to the vertical flux above the canopy (e.g. Shuttleworth and Wallace, 1985). Combination of Eqs.11 and 13 allows the unknown q_o to be eliminated and, with r_{st} replaced by r_s, yields

$$\lambda E_o = \rho\lambda(q^*(T_o) - q_a)/(r_{aV} + r_s) \tag{15}$$

where λ is the latent heat (units of Jkg^{-1}). For closed canopies, where E_o is predominantly transpiration, experimental results support the use of r_{st} in Eq.15. These show that r_{st} depends on several environmental factors, with a strong diurnal variation, as well as varying between species.

(b) Surface energy balance and radiative fluxes

Calculation of the fluxes requires knowledge of the surface temperature. Determination of this is based on the surface energy balance, written as

$$R_{No} - G_o = H_o + \lambda E_o \tag{16}$$

Here R_{No} is the net radiative flux density to the surface (net radiation) and G_o is the heat flux into the soil; the sum of the fluxes on the LHS of Eq.16 defines the available energy. The flux G_o is to be interpreted as the soil heat flux at the surface, and can be calculated from consideration of heat conduction and conservation in the soil. The heat conservation equation for a homogeneous soil in the absence of heat sources and sinks can be written

$$\rho_s c_s \frac{\partial T_s}{\partial t} = -\frac{\partial G}{\partial z} \tag{17}$$

where,

$$G = -k_s \frac{\partial T_s}{\partial z}. \tag{18}$$

In the above, $C_s = \rho_s c_s$ is termed the volumetric heat capacity (units of $Jm^{-3}K^{-1}$), ρ_s is the soil density and c_s is the soil specific heat. In addition, k_s is the thermal conductivity of the soil, where $k_s = \rho_s c_s \kappa_s$, and κ_s is the thermal diffusivity. Combining Eqs.17 and 18 yields the heat conduction equation,

$$\frac{\partial T_s}{\partial t} = \kappa_s \frac{\partial^2 T_s}{\partial z^2}. \tag{19}$$

In finite difference form, this can be solved numerically in a multilevel soil model to give $T_s(z,t)$ and hence G_o from Eq.18.

Alternatively, Eq.16 can be rewritten as a rate equation for the surface temperature. The relation between G_o , the surface soil heat flux, and G_1 the heat flux at a small depth in the soil follows from Eq.17

$$\rho_s c_s \Delta z' \frac{\partial T_s}{\partial t} = \frac{\partial W_s}{\partial t} = G_o - G_1. \tag{20}$$

This allows Eq.16 to be written as,

$$R_{No} - G_1 = H_o + \lambda E_o + C_g \frac{\partial T_s}{\partial t} \tag{21}$$

where $C_g \partial T_s/\partial t$ is the rate of energy storage per unit area in the thin soil layer. Eq.16 contains the net radiation which, with the adopted sign convention, is generally positive by day and negative at night over land. R_{No} contains a combination of shortwave and longwave fluxes, such that

$$R_{No} = R_{so}(1 - \alpha_s) + \epsilon_s R^d_{Lo} + R^u_{Lo} \tag{22}$$

where R_{so} is the global shortwave radiative flux (positive), R^d_{Lo} is the downward longwave flux (positive) and R^u_{Lo} is the upward longwave flux (negative), all at the surface. In addition, α_s is the shortwave albedo of the surface and ϵ_s is its longwave emissivity. In Eq.22, we have allowed for an amount $(1 - \epsilon_s)R^d_{Lo}$ of reflected longwave radiation, which equals zero if the surface is a blackbody with $\epsilon_s = 1$.

(c) Surface temperature

Numerical models of the atmosphere usually compute the ground surface temperature (T_o) from either Eq.16 (a diagnostic form of the SEB equation) or from Eq. 21 (a prognostic form of the SEB equation, i.e. a rate equation for T_o).

1. Diagnostic Solutions.

In the diagnostic case, ground heat flux may be parameterized very crudely - e.g. as a constant fraction of R_N or by assuming the heat capacity of the ground is zero and setting $G_o = 0$. Alternatively, it may be computed using a full treatment of soil heat diffusion in a multi-level soil model (Eq.19).

All of the terms in Eq.16 are either computed separately or parameterized in terms of T_o , and the equation is solved iteratively using the Newton-Raphson method, for example.

2. Prognostic Solutions.

In the prognostic case (Eq.21), soil heat flux G_1 may be crudely parameterized or even set to zero (the so-called 'Forcing Method'). One method which is widely used determines G_1 from a two-layer soil model (the so-called 'Force Restore Method'). In this, the surface temperature (T_o) is approximated by the temperature of the thin upper layer, of temperature T_s and thickness $\Delta z'$. The deeper soil layer is assumed to be of sufficent depth (d'_1) that over time scales of interest the flux of heat at the bottom is zero (see Section 4).

(d) Surface humidity and soil moisture

The level of soil moisture is closely linked with the evaporation from the soil surface, and governed by the mass water balance in a surface layer of soil, depth d. For a unit area of surface, the balance can be written

$$\rho_w d \frac{\partial \eta}{\partial t} = \rho_w P - E_o - F_{wd} \tag{23}$$

where ρ_w is the density of water, η is the soil moisture content (units of volume per unit volume), P is the precipitation rate (units of velocity) and F_{wd} is the flux of water across the base of the layer.

In determining the surface humidity for a bare soil surface, two quite different approaches need to be identified - interactive and non-interactive. The non-interactive approach means that the surface humidity or soil wetness does not respond to atmospheric forcing in a realistic way, if at all.

1. Non-Interactive (Diagnostic) Schemes.

The evaporation from, and hence the surface temperature of, a bare soil surface is highly dependent on the surface humidity, and thus upon the near-surface soil moisture content. The problem of computing q_o (or the surface relative humidity, h_o) for a bare soil has been bypassed in many numerical models of the atmosphere by specifying some measure of the surface wetness. For some purposes this may be acceptable, but mostly it is at best a very crude representation of the evaporation process and, in particular, fails to include properly the feedback between the atmosphere and surface moisture status. Two examples of non-interactive schemes are given below.

(i) The actual evaporation is set to a constant fraction (x) of the potential evaporation E_p , viz.

$$E = xE_p. \tag{24}$$

This implies (Eqs.11 and 12),

$$q_o = xq_o^*(T_o) + (1 - x)q_a \tag{25}$$

where T_o is the temperature of the drying soil surface. It should be noted that a more practicable temperature is T_{op} , the temperature that the surface would have if it were actually wet, and q and T held constant. However, this hypothetical temperature is unknown and the use of T_o in Eq.12 will result

in unrealistically high values of E_p when the surface is dry. The problem can be partly solved by using the scaling evaporation E_l in place of E_p . This is given by the Penman-Monteith combination equation (Garratt, 1991), written here as

$$\lambda E_l = \Gamma(R_N - G_o) + (1 - \Gamma)\rho\lambda\delta q_a / r_{aV} \qquad (26)$$

where $\Gamma = s/(s+\gamma)$, s is $\partial q^*/\partial T$, $\gamma = c_p/\lambda$ the psychrometric constant, and δq_a is the humidity deficit in the air. For a wet surface $E_l = E_p$. In Eq.25, an undesirable feature from a conceptual viewpoint is the dependence of q_o on q_a, the specific humidity at the first atmospheric level and thus an implicit dependence on the choice of reference level.

(ii) The surface relative humidity is set to a constant value, viz. $h_o = q_o/q_o^*(T_o) = constant$.

For many purposes, it is necessary to employ an interactive scheme with a realistic dependence of E upon soil moisture, but one which is less detailed than a multi-level soil model approach based on solution of the 1D moisture diffusion equations.

2. Interactive Schemes.

One very simple approach is to set the surface relative humidity to a simple function of soil moisture, e.g. $h_o = \eta_g/\eta_s$, as done in the standard version of the two CSIRO models. In this, η_g is calculated using Method 2 below.

More generally, in Eq.24, x is made to depend on soil moisture status according to two approaches involving the moisture content of either a thick upper layer of soil (Method 1) or that of a thin near-surface layer of soil (Method 2).

(i). Method 1 ('Bucket').

In this approach (Fig.5), x is given by

$$x = min(1, \eta_{bb}/\eta_k) \qquad (27)$$

where η_{bb} is the volumetric moisture content of the soil layer of depth d_2 and η_k is a critical value; for $\eta_{bb} > \eta_k$ the surface behaves as if it were saturated. This is only one of many expressions for x; in fact, experiments have never given a consistent form for x dealing, as they do, with real soils. That is the major limitation of Eqs.24 and 25; the main virtue of this approach is its simplicity, giving values of evaporation constrained between wet and dry limits.

At depth d_2 , the moisture flux is taken to be zero, so from Eq.23

$$\frac{\partial \eta_{bb}}{\partial t} = \frac{(P - E/\rho_w)}{d_2}. \tag{28}$$

Here, $0 \leq \eta_{bb} \leq \eta_s$, where η_s is the maximum (saturation) value above which runoff is assumed to occur. For time scales of a few days, d_2 in the range 0.5 to $1m$ is a typical value used in numerical models, with $\eta_k \approx 0.75\eta_s$. For longer time scales, drainage out through the bottom of the layer may become significant though it is often ignored or assumed to be part of the general runoff.

The main shortcoming of Eqs.24, 27 and 28 is that E does not respond rapidly to short-period occurrences of precipitation, which rather change η_{bb} and hence E only gradually.

(ii) Method 2 ('Force Restore').

Near-surface soil moisture (η_g) can be treated in an analogous way to that of surface temperature using a two-layer soil model. As with temperature, the model must represent both the rapid response of the near-surface moisture to forcing by precipitation or evaporation and also provide a source of moisture from the deep soil to the surface when there is no precipitation (see Section 3).

(e) Canopy parameterization

The presence of vegetation over an area of ground modulates the evaporation from the soil, and contributes further to the vertical flux of water vapour into the ABL through transpiration. A realistic canopy formulation must ultimately represent the effects of vegetation (averaged over the grid square in a 3D numerical model) upon evaporation, energy partitioning, rainfall interception and soil moisture, as well as albedo and aerodynamic roughness. Inclusion of canopy effects allows the deep soil moisture (in the root zone) to act as a source for evapotranspiration. Except when completely wet, the canopy foliage will exert some degree of physiological control upon the evaporation rate, and the surface humidity becomes indeterminate. Under these conditions, a canopy or surface resistance is introduced into the evaporation formulation, and the resistance concept is at the heart of most canopy models.

Single-level, canopy models are most appropriate for use in mesoscale and general circulation models, and these will be emphasised here. GCMs, for example, can have the option of full canopy or bare soil grid coverage. For

partial canopy cover, either as a sparse uniformly distributed cover or as full cover occupying only a fraction of the grid area, more complexity is involved.

For a complete vegetation cover, the simplest canopy model uses a constant r_s in Eq.15 for evaporation, with r_s values consistent with known bulk stomatal resistances, together with the specified albedo and z_o . In contrast, a complex single-level canopy model (SiB, BATS) may contain a large amount of detail with which to evaluate fluxes from the soil beneath the canopy, from open areas between the canopy elements as well as from the foliage itself. In addition the component fluxes will be averaged over the grid area in some realistic way. With this approach, quite sophisticated treatments for the surface resistance may be used (see Section 5).

Phase 1 of the biospheric submodel planned for the CSIRO DAR GCMs consists of a simple, but realistic, soil/canopy scheme based on the work of Deardorff (1977, 1978) and Noilhan and Planton (1989). In the GCMs, two options are available. The first assumes the canopy layer and top soil layer are at the same temperature (the isothermal approach) so that a single surface temperature at the model grid point is evaluated. The second option assumes that the grid area comprises a fraction of dense canopy (σ_f) where the temperature is calculated separately from the soil surface temperature comprising a fraction $(1 - \sigma_f)$. The scheme has been tested and calibrated independently by the use of a 1D stand-alone model, which consists of a two-layer soil scheme ('force-restore' for temperature and moisture) and canopy formulation coupled to the essential elements of the CSU mesoscale model (viz. dynamics, radiation, boundary-layer depth e.g. as used in Garratt et al., 1990). The soil and canopy schemes are described in this technical paper, together with the results of comparisons between the 1D model, the mesoscale model in 1D form utilising a multilevel soil moisture and heat diffusion scheme, and observations of fluxes over vegetation.

3 Two layer soil moisture scheme

(a) Formulation

In GCMs, a realistic representation of soil moisture availability and its long term evolution is required. However, this has to be modelled with the simplest method consistent with the complexity of other parameterization schemes used. Early GCM models used a simple parametrization of soil

moisture known as the 'bucket' method, (Manabe, 1969). The evolution of soil moisture in a single slab is given by a prognostic equation incorporating precipitation, evaporation, and runoff. The method generally overestimates the near-surface moisture content for drying soils (Laval, 1988). Deardorff (1977) proposed a 'force restore' scheme where the soil is represented as a double layer with a diffusion type exchange between the moisture of an upper thin layer and the bulk moisture of a deep bottom layer. Both layers are of constant depth. His equation for the surface moisture content η_g is:

$$\frac{\partial \eta_g}{\partial t} = -C_1 \frac{(E_g - P\rho_w)}{\rho_w d_1} - C_2 \frac{(\eta_g - \eta_2)}{\tau} \tag{29}$$

where E_g is ground evaporation, P is precipitation, ρ_w is the density of liquid water, τ is one day, d_1 is the depth to which the diurnal soil moisture cycle extends and η_2 is the vertically averaged soil moisture of the thicker layer. Deardorff's time dependent equation for bulk moisture is:

$$\frac{\partial \eta_2}{\partial t} = -\frac{(E_g - P\rho_w)}{\rho_w d_2}. \tag{30}$$

Deardorff's scheme was modified by Noilhan and Planton (1989), to include the effects of gravity on the near-surface moisture. The equations for soil moisture in our one dimensional stand-alone model are based on these earlier works, and can be written as follows. For η_g :

$$\frac{\partial \eta_g}{\partial t} = -C_1 \frac{E_g - (P\rho_w + M_s\rho_{snow} - R\rho_w)}{\rho_w d_1} - C_2 \frac{(\eta_g - \eta_{eq})}{\tau} \tag{31}$$

where η_{eq} is the volumetric moisture of the thick layer when the gravity force balances the capillarity and adhesive forces, and we have set $d_1 = 0.1m$. The use of η_{eq} rather than η_2 as in Deardorff's scheme is preferable as soil moisture flux (W_s) is a function of the matrix potential (ψ_η) representing the work required to extract water against capillarity and adhesive forces, gravitational head (z) and hydraulic conductivity (K_η) accounting for gravity drainage, i.e.:

$$W_s = K_\eta \rho_w \frac{\partial(\psi_\eta + z)}{\partial z} \tag{32}$$

and soil moisture content:

$$\rho_w \frac{\partial \eta_g}{\partial t} = -\frac{\partial W_s}{\partial z}. \tag{33}$$

Noilhan and Planton (1989) calculated η_{eq} as a function of the mean moisture for three soil types. With the exception of sand, η_{eq} differs significantly from η_2 only for moisture near saturation. In the case of soils with a coarse texture, like sand, the capillarity and adhesive forces are very small and water diffuses quickly under the gravity force, hence the equilibrium values are lower than the initial mean moisture.

The first term in (31) is a forcing term; it describes the effects of fluxes of water at the surface i.e. drying when evaporation (E_g) or runoff (R) occurs or wetting when rainfall (P) or snowmelt (M_s) occurs. The second term tends to restore surface moisture to its bulk value. The equation describing the water budget in the bottom layer is:

$$\frac{\partial \eta_2}{\partial t} = C_2 \frac{d_1}{d_2} \frac{(\eta_g - \eta_{eq})}{\tau}. \tag{34}$$

The term on the right hand side of Eq. (34) is proportional to the difference between surface moisture and equilibrium moisture and it characterizes the flux of water entering or leaving the deep layer. Depth d_2 must be sufficiently large so that the drainage at the bottom of this layer is negligible; we set $d_2 = 1m$. The formulation (34) is to be prefered to (30); for example, after rain, η_2 will still increase due to a high value of η_g rather than decrease due to evaporation.

Coefficients C_1 and C_2 are dependent on the physical properties of the soil and moisture. In Deardorff (1977) they were estimated from one set of experimental field data. In Noilhan and Planton (1989), the coefficients C_1 and C_2 were determined with a 26 layer hydrological model for a range of soil conditions. The moisture scheme in the 1D S/A model uses values of C_1 and C_2 determined from the CSU mesoscale model run in 1D mode, which incorporates a multilayer soil moisture diffusion scheme, involving quantities such as the saturated and wilting moisture content, hydraulic conductivity and the moisture potential. The model has 14 levels in a 1m thick soil layer. The CSU model utilises a range of soil types (12), with the physical properties of soil as described and classified by Clapp and Hornberger (1978) and Cosby et al. (1984), (see e.g. McCumber and Pielke, 1981).

(b) Computation of C_1 and C_2 coefficients

Coefficients C_1 and C_2 represent the hydraulic properties of the soil as a function of soil moisture. The multilayer moisture scheme in the CSU mesoscale model was used to evaluate C_1 and C_2 for three types of soil and a range of moistures.

Rewriting Eq.(31) (without the downwards water fluxes) in a finite difference form for day and night conditions we obtain:

$$\begin{aligned} \Delta\eta_{g,day} &= C_1' E_{day} + C_2'(\eta_g - \eta_{eq})_{day} \\ \Delta\eta_{g,night} &= C_1' E_{night} + C_2'(\eta_g - \eta_{eq})_{night} \end{aligned} \tag{35}$$

and

$$\begin{aligned} C_1' &= \Delta t C_1/(\rho_w d_1) \\ C_2' &= \Delta t C_2/\tau. \end{aligned}$$

From the mesoscale model calculations $\Delta\eta_g$, E and $(\eta_g - \eta_{eq})$ are known and C_1' and C_2' can be solved for each two hour period from:

$$C_1' = \frac{\Delta\eta_{g,day}(\eta_g - \eta_{eq})_{night} - \Delta\eta_{g,night}(\eta_g - \eta_{eq})_{day}}{E_{day}(\eta_g - \eta_{eq})_{night} - E_{night}(\eta_g - \eta_{eq})_{day}} \tag{36}$$

$$C_2' = \frac{\Delta\eta_{g,day} E_{night} - \Delta\eta_{g,night} E_{day}}{E_{night}(\eta_g - \eta_{eq})_{day} - E_{day}(\eta_g - \eta_{eq})_{night}}.$$

The set of discrete values of C_1 coefficients was fitted using the least square method, for a range of soil moisture conditions. Figure 3 illustrates variations of C_1 as a function of soil moisture for 3 soil types. C_1 is inversly proportional to hydraulic diffusivity D_η which is a function of hydraulic conductivity K_η, and matrix potential ψ_η. The smallest value of C_1 corresponds to a high value of moisture when potential evaporation occurs. As the soil dries out, the evaporation decreases until the moisture falls below the wilting value around which C_1 rapidly increases.

The value of C_2 describes the restoration of the soil moisture to its equilibrium value. Numerical experiments showed that any C_2 variation had an insignificant effect on the soil moisture, hence constant values were chosen for each soil type. Figure 4a summarises the variation of C_1 with fractional moisture content and Fig. 4b the variation of C_2 with moisture content, as determined by other workers i.e. Deardorff, (1977), Noilhan and Planton (1989), and Toya and Yasuda, (1988).

Formulae for C_1 and C_2 adopted for the 1D S/A model are as follows, where $t = \eta_g/\eta_{sat}$:

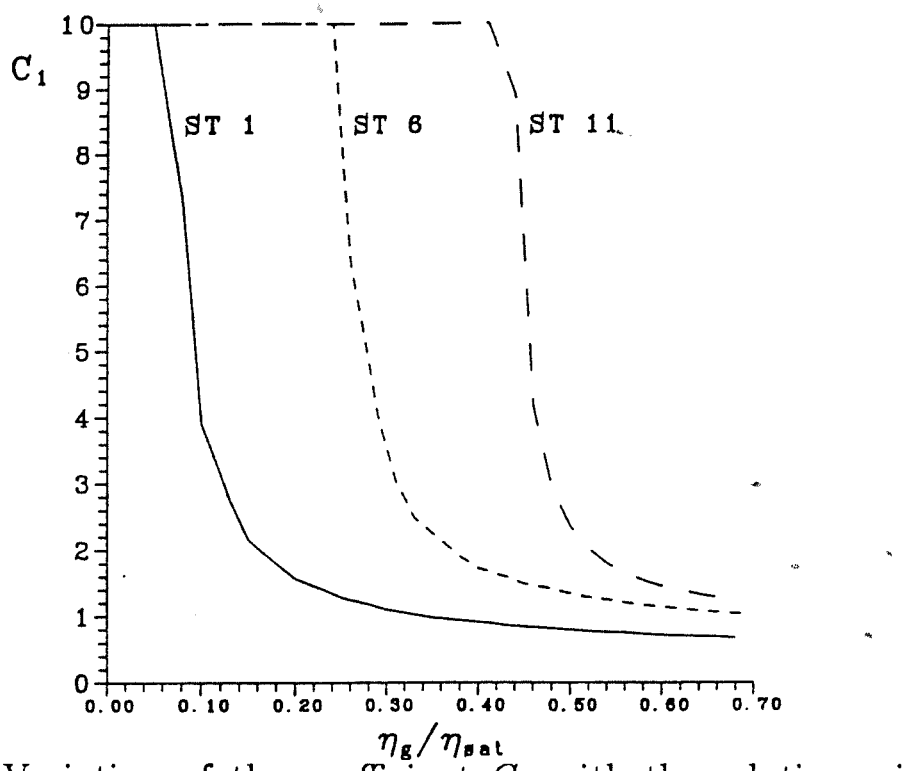

Figure 3: Variation of the coefficient C_1 with the relative soil moisture content for three soil types, based on numerical simulations in an interactive soil-atmosphere model.

sand

$$C_1 = \begin{cases} 10 & \text{if } t \leq 0.05 \\ (1.80t + 0.962)/(5.0t + 0.200) & otherwise \end{cases} \qquad C_2 = 2.0$$

sandy clay loam

$$C_1 = \begin{cases} 10 & \text{if } t \leq 0.226 \\ (1.78t + 0.253)/(2.96t - 0.581) & otherwise \end{cases} \qquad C_2 = 3.0$$

clay

$$C_1 = \begin{cases} 10 & \text{if } t \leq 0.421 \\ (2.22t - 0.556)/(2.78t - 1.114) & otherwise \end{cases} \qquad C_2 = 1.9$$

(c) Modelling evaporation from the ground

In most GCM models, ground evaporation is modelled as a fraction of a potential evaporation with a proportionality factor depending on the ratio of moisture at the surface to the saturation moisture:

$$E_g = f(\frac{\eta_g}{\eta_{sat}})E_p \tag{37}$$

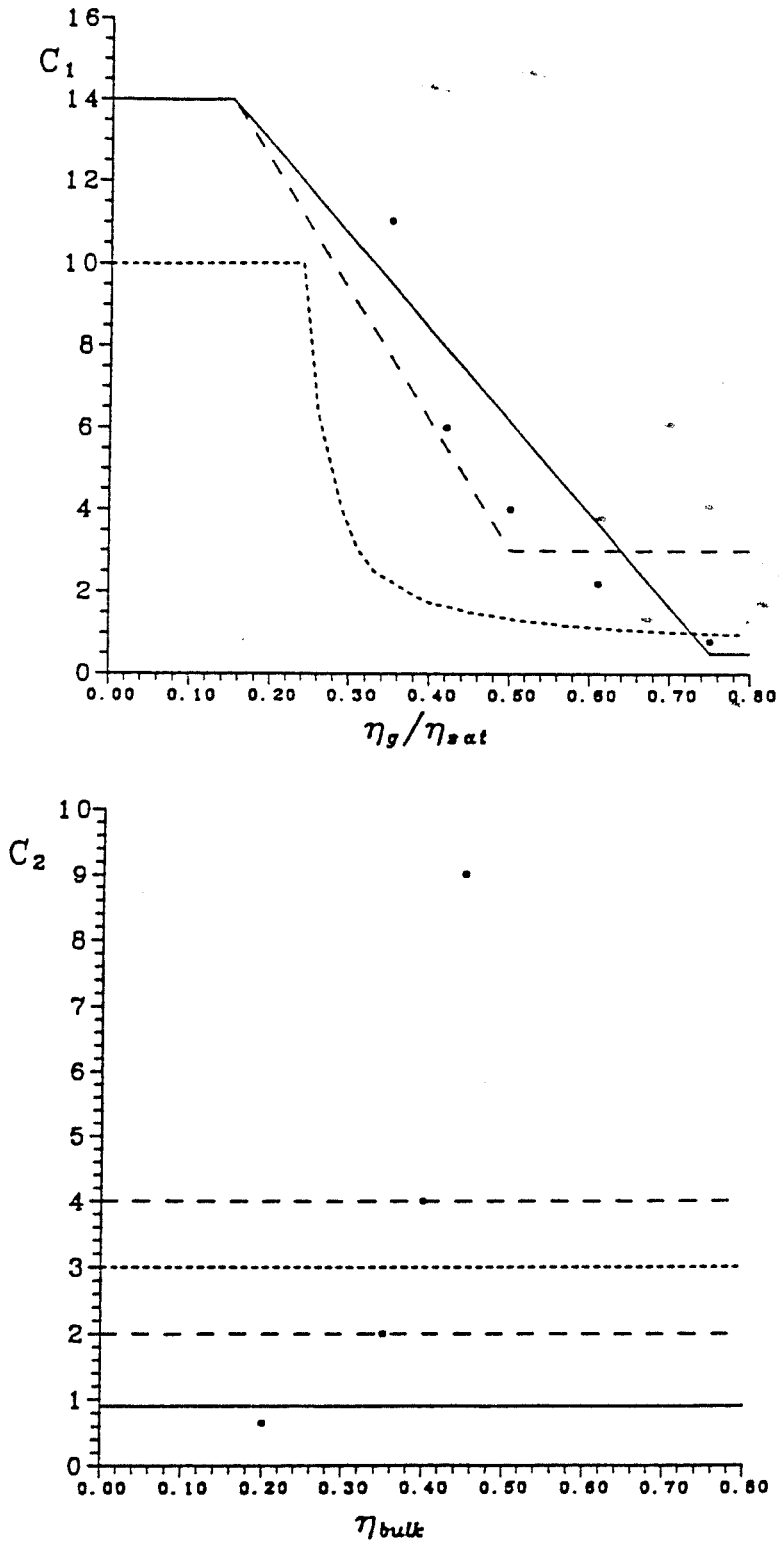

Figure 4: (a) Variation of the coefficient C_1 with the relative soil moisture content for soil type 6, comparison with other determinations for medium soils. Continuous line - Deardorff (1977); long-pecked lines - Toya & Yasuda (1988); full circles - Noilhan & Planton (1989). (b) As in (a), for C_2 versus the bulk moisture content.

where E_p is given either by Eq.(12) or (26) (with $E_p = E_l$). Mesoscale model simulations for a range of soils and soil moisture conditions were used to evaluate the function f with E_l based on Eq. (26). Figure 5 illustrates the data for sand, loam and clay. Such a relationship between actual and potential evaporation has been demonstrated in the analyses of Priestley & Taylor (1972) and Mahrt & Pan (1984), based on observations and numerical model results. Simulations covered a range of climatic conditions (hence the scatter in the plotted data), and mean straight lines were drawn by eye to represent the results.

Formulae for $f(\eta_g/\eta_{sat})$ were adopted as follows, with $t = \eta_g/\eta_{sat}$:

sand

$$f(t) = \begin{cases} 1 & \text{if } t \geq 0.15 \\ 11.49(t - 0.063) & \text{if } 0.063 \leq t < 0.15 \\ 0 & \text{if } t < 0.063 \end{cases} \tag{38}$$

sandy clay loam

$$f(t) = \begin{cases} 1 & \text{if } t \geq 0.365 \\ 6.90(t - 0.220) & \text{if } 0.22 \leq t < 0.365 \\ 0 & \text{if } t < 0.22 \end{cases}$$

clay

$$f(t) = \begin{cases} 1 & \text{if } t \geq 0.52 \\ 8.33(t - 0.40) & \text{if } 0.4 \leq t < 0.52 \\ 0 & \text{if } t < 0.40 \end{cases}$$

In the case of sand, which has a low wilting value, evaporation is essentially potential for moistures above 0.0677. Clay has a high wilting value of 0.286 and evaporation is close to potential only for high surface moisture.

(d) Validation

One of the difficulties in validating a parameterization scheme is obtaining experimental data on the required time and space scale. In the case of the two layer soil model, validation is based on a comparison with results of the multilayer scheme in the mesoscale model.

Seven day simulations of the soil moisture content, and its time evolution, were compared for the 3 soil types but only the results for sandy clay loam

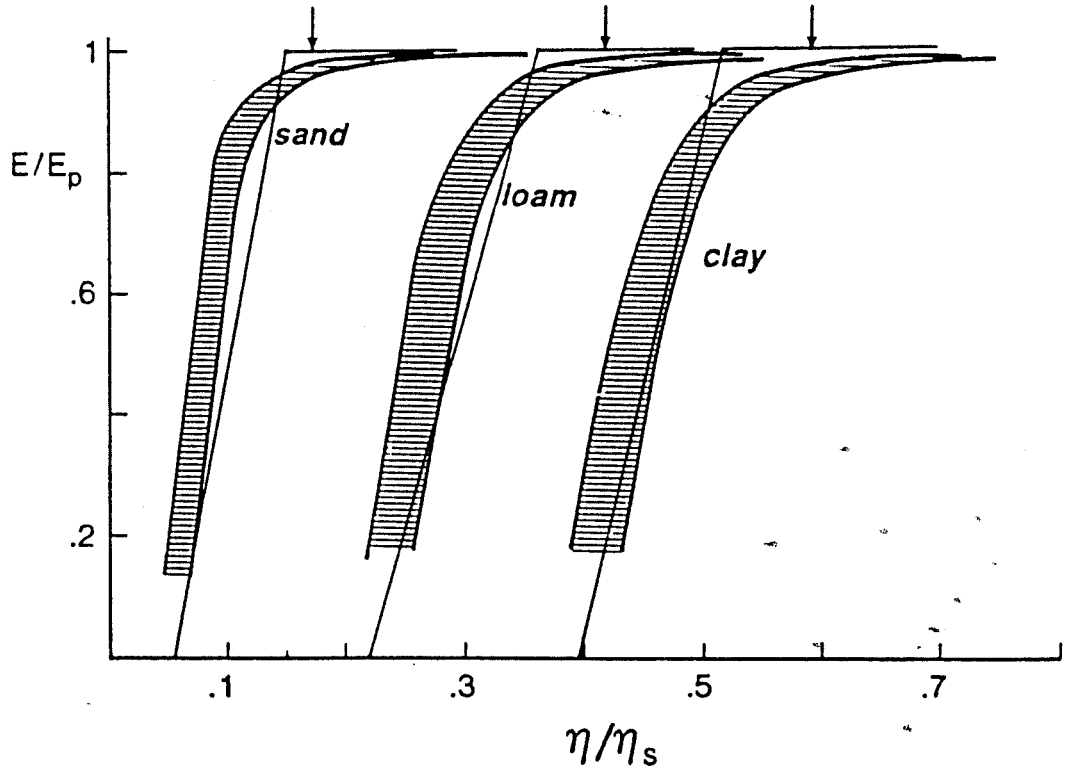

Figure 5: E/E_p (E_p from Eq. 26) as a function of the relative soil moisture content, based on numerical simulations for three soil types in an interactive soil-atmosphere model. Simulations have been done for a range of climate conditions (mid-latitude summer) represented by the shaded regions (the temperature range is 283 to 303K and $q = 0.005$).

(soil type 6) are shown here. For a high value of moisture, see Fig. (6a), the diurnal variation of latent heat flux is predicted correctly. As soil dries, see Fig. (6b), evaporation decreases at a lesser rate in the 1D S/A model, evidently related to the linear approximation of E/E_p upon soil moisture used in the 1D S/A model. For example, for moisture just below the wilting value (see Fig. 6b, day 1), the mesoscale model has reduced evaporation already, while the 1D S/A model still gives evaporation at the potential rate. After six days both models have essentially the same reduced evaporation. For dry soil, Fig. (6c), evaporation is very low and the daily moisture variation small.

Similar behaviour for a drying soil condition is observed for sand and clay (soil types 1 and 11), see Fig. (7). Evaporation is close to the potential rate at day one and gradually decreases as the soil dries.

The above results indicate that the two layer model is able to simulate correctly the latent heat flux as a function of soil moisture and the soil moisture time evolution for the three soil types modelled here.

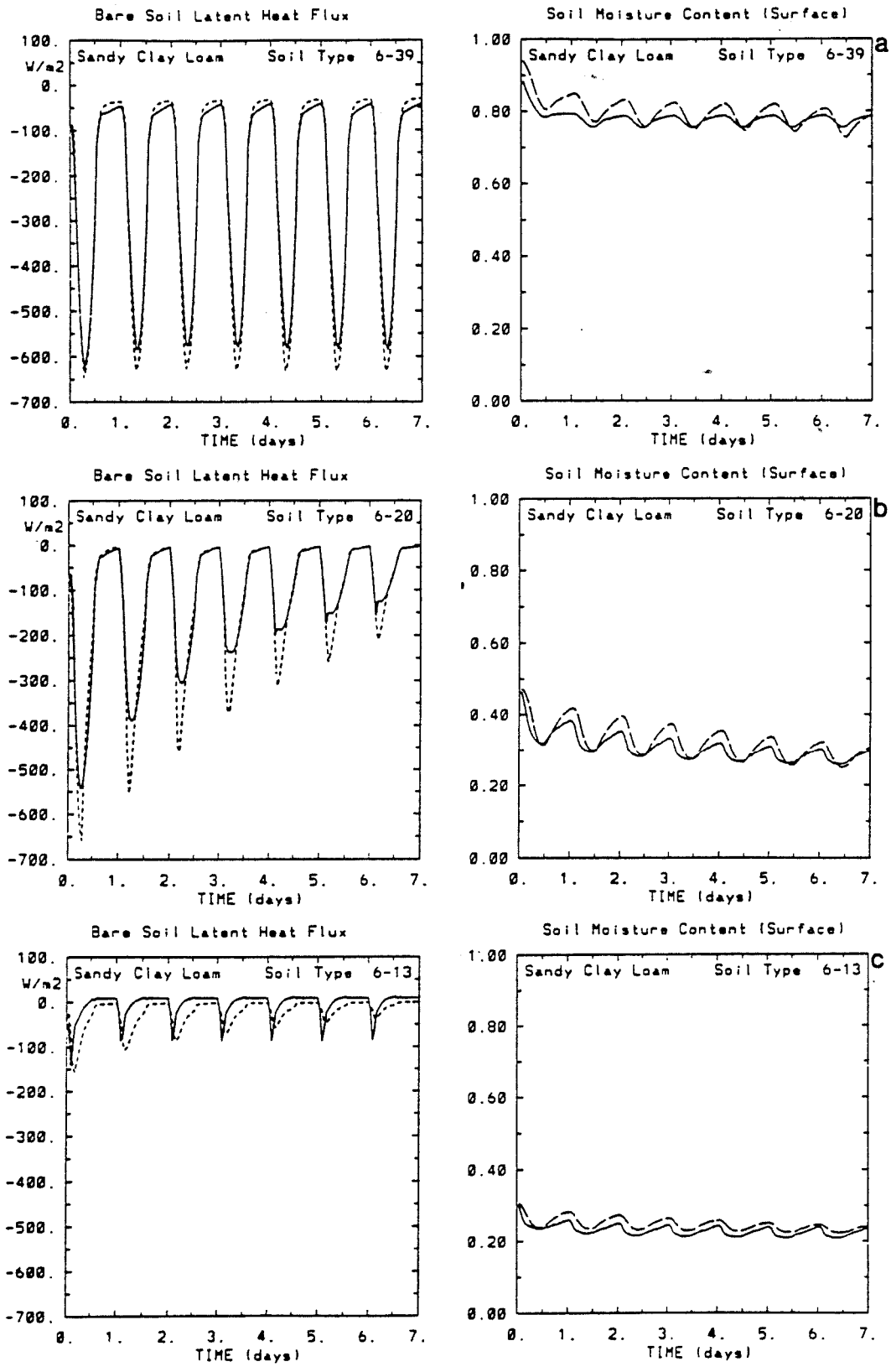

Figure 6: Variations of the latent heat flux and near-surface moisture content over a period of 7 days based on simulations in the full 1D mesoscale model with multi-layer soil scheme (solid curve) and the 1D stand-alone model (short pecked curve). The diagram shows results for soil type 6, with initial soil moisture contents of 0.4 (a), 0.2 (b) and 0.13 (c).

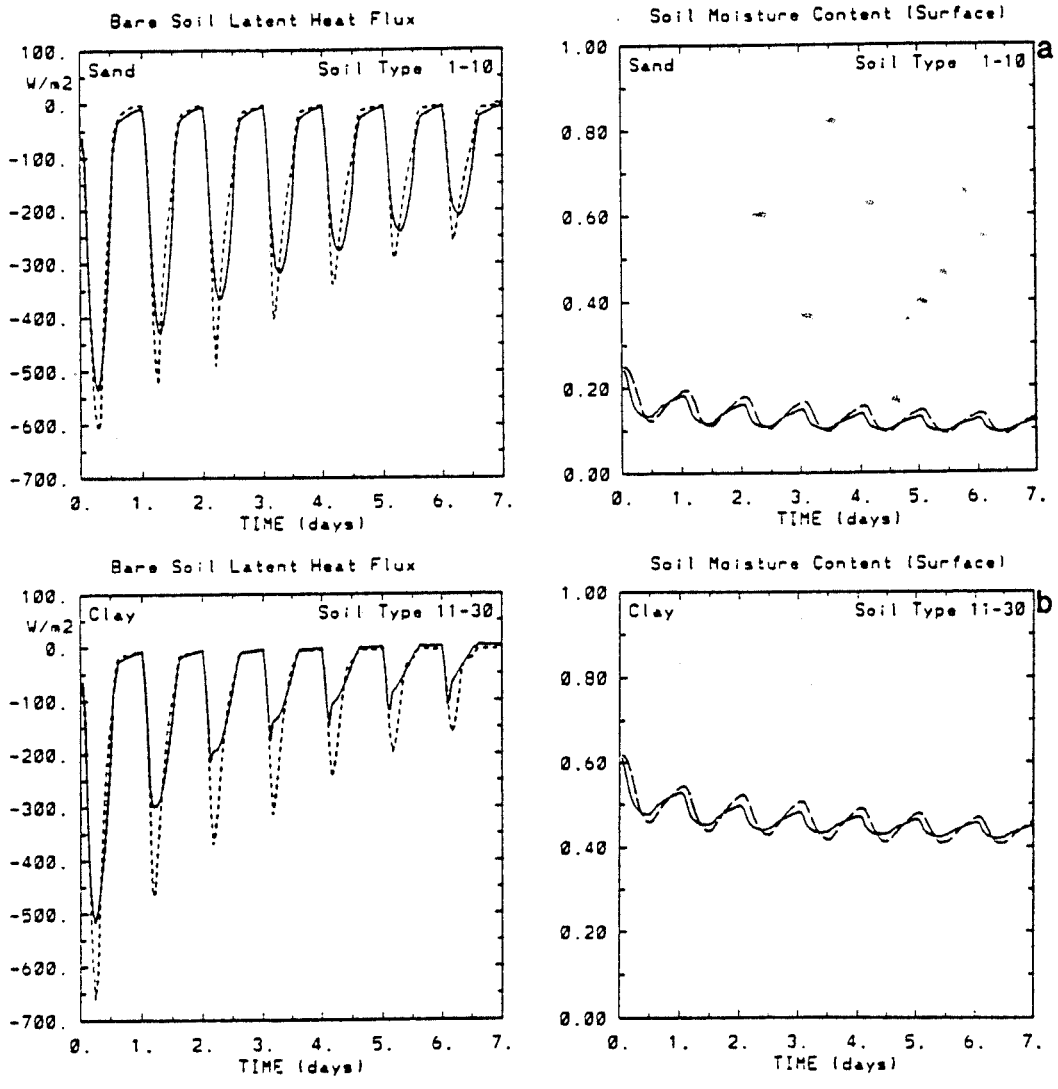

Figure 7: As in Fig.6, for drying soils only - soil type 1 with initial moisture content of 0.1 (a) and soil type 11 with initial moisture content of 0.3 (b).

4 Two layer soil temperature scheme

A time dependent 'force-restore' method for the evaluation of soil temperature is used in the 1D S/A model. It is based on the work of Bhumralkar (1975) and Blackadar (1979). The temperatures of a thin surface layer related to a scaling depth d_1', and of a deeper thick layer of physical depth d_2' (acting as a heat reservoir) are determined from (cf. Eq. 21):

$$\frac{\partial T_g}{\partial t} = -c_1 \frac{H_A}{\rho_s c_s d_1'} - c_2 \frac{T_g - T_b}{\tau} \tag{39}$$

$$\frac{\partial T_b}{\partial t} \approx -\frac{H_A}{\rho_s c_s d_2'} \tag{40}$$

where the heat flux into the soil $H_A = -G_0$ is given by Eq.(16). Values of the coefficients in Eq. 39 are taken as $c_1 = 3.72$ and $c_2 = 7.4$, and depths are calculated using:

$$d_1' = (\kappa_s \tau/\pi)^{1/2} \tag{41}$$

$$d_2' = (365\kappa_s \tau/\pi)^{1/2}. \tag{42}$$

The thermal parameters are functions of soil moisture, with

$$\begin{aligned} \kappa_s &= k_s/\rho_s c_s \\ \rho_s c_s &= (1-\eta_{sat})\rho_{s,dry} c_{s,dry} + \eta \rho_{water} c_{s,water} \\ k_s &= 419(a\,\eta_g + b\,\eta_g^{0.4}). \end{aligned}$$

and a and b depending on soil type i.e., for sand $a = 0.004$ and $b = 0.006$, for sandy clay loam $a = 0.003$ and $b = 0.004$ and for clay $a = 0.002$ and $b = 0.003$. The thermal conductivity, k_s, varies by about one order of magnitude as the soil dries out. Hence depths d_1' and d_2' are approximately $0.06m$ and $1.1m$ respectively for dry soils, while being between 0.1 to $0.2m$ and 2.0 to $5.5m$ respectively for wet soils.

Deardorff (1978) compared five approximate methods (including 'force-restore') for the calculation of soil temperature with a 12-layer soil model. The 'force-restore' method was found to give the best approximation to the diurnal cycle of surface temperature, especially for large time steps of 10 to 30 min typically used in GCM models.

The temperature of the surface depends primarily on the net radiation and the fluxes, both molecular and turbulent, transporting heat to/from the surface. This dependence is described by the first term in Eq.(39) i.e. the forcing term where individual flux components are dependent on the temperature gradient between the surface and the atmosphere (Eq. 10 and 11), and the surface and soil layers beneath the surface. The second term in Eq. (39) describes the restoration of surface temperature towards its deep layer value.

Here, the seven day simulation results for 3 soil types are presented. First, for wet soil (sandy clay loam), see Fig. (8a) and (6a), the latent heat flux is large, so less energy is available to heat the soil, resulting in a cooler soil surface and small daytime sensible heat fluxes. For dry soil, see Fig. (8c) and (6c), the evaporation is small and energy is used to warm the soil, giving a high soil temperature and large daytime sensible heat fluxes. For drying soil, see Fig. (8b), the diurnal amplitude of soil temperature increases from 30°C on day one to approximately 50°C on day seven. Similar behaviour is observed for sand and clay (soil types 1 and 11), see Fig(9). The maximum temperature for soil type 11 on day seven approached 335K, (62°C). Such values are realistic and have been observed over dry surfaces under high insolation (e.g. Garratt, 1992b). To demonstrate the capacity of the 1D S/A model to generate extreme diurnal amplitude in soil temperature, Fig.(10) shows results for a two day simulation with the 1D S/A and 1D mesoscale models, where insolation is high near the summer solstice. The surface is dry clay, with an albedo of 0.15 and the initial atmospheric temperatures some 25K above the climatological mean vertical profile for the latitude. Under such conditions we were able to generate a maximum screen-level air temperature of 55°C, close to the highest ever observed, together with a maximum surface temperature close to 90°C. This is slightly in excess of reported extreme soil temperatures of 80 to 85°C (Garratt,1992b).

It is clear from the above results that the dominant influence of soil moisture content upon soil temperature and fluxes is reproduced.

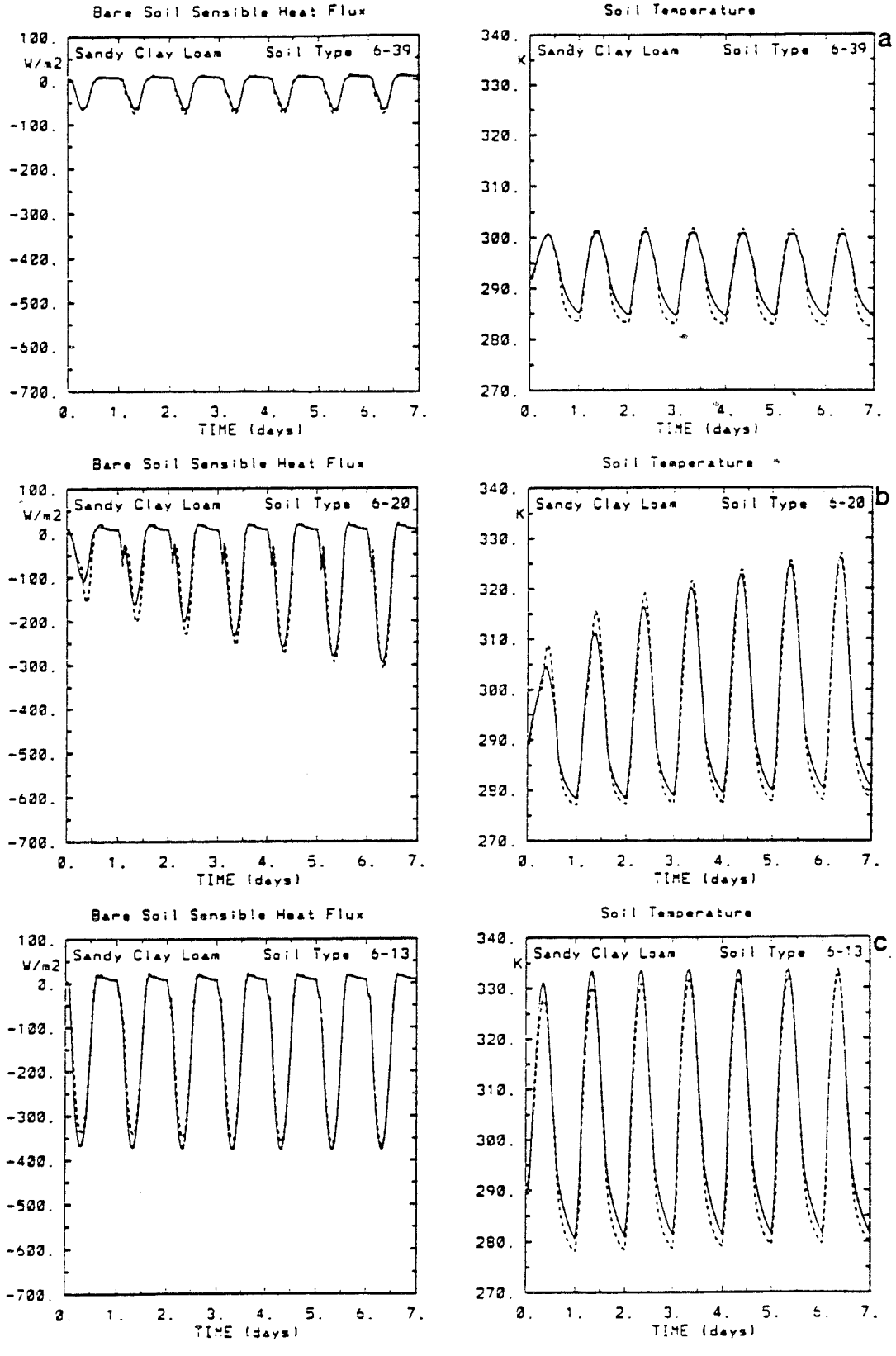

Figure 8: Variations of the sensible heat flux and surface temperature over a period of 7 days based on simulations in the full 1D mesoscale model with multi-layer soil scheme (solid curve) and the 1D stand-alone model (short pecked curve). For soil type 6, with initial soil moisture contents of 0.4 (a), 0.2 (b) and 0.13 (c).

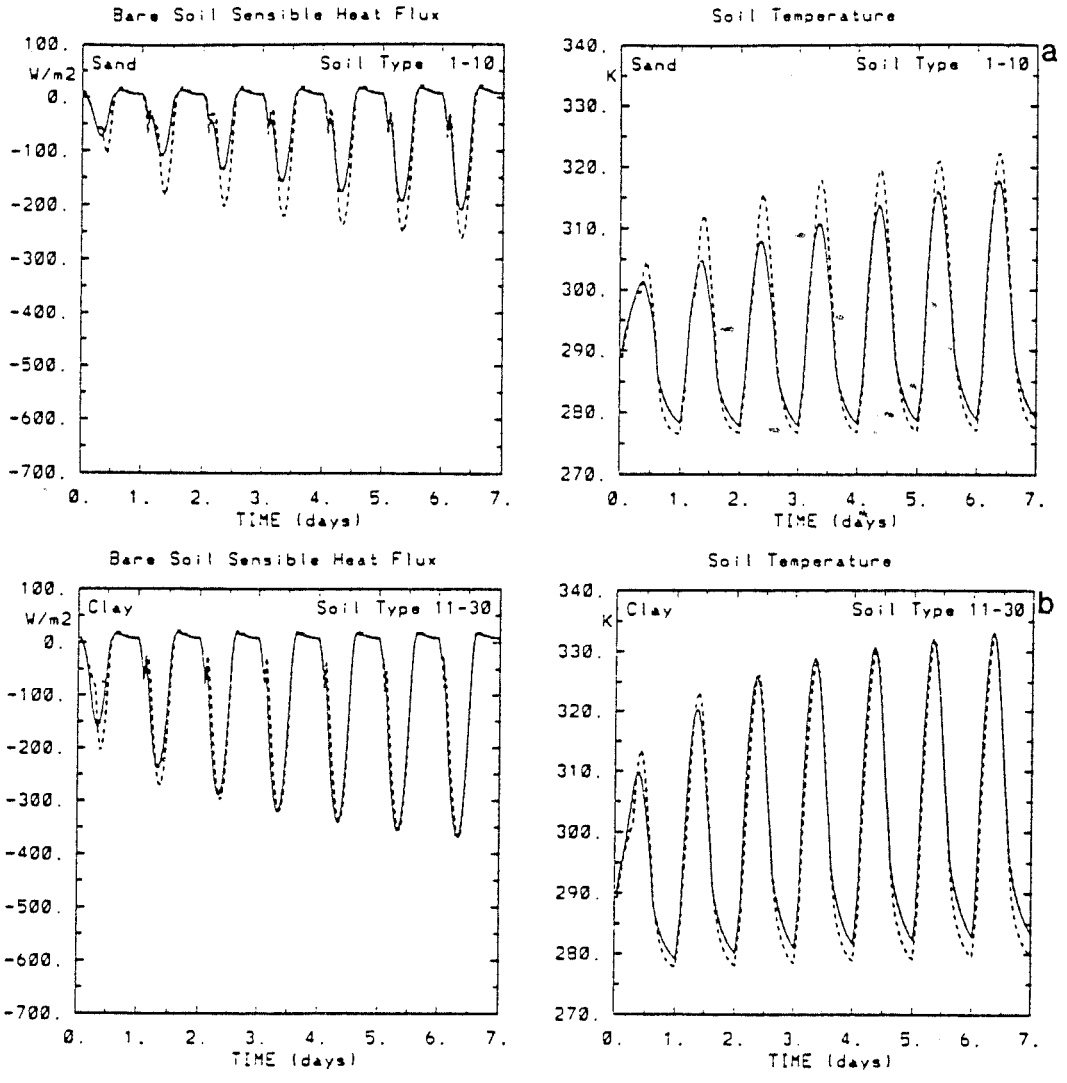

Figure 9: As in Fig.8, for drying soils only - soil type 1 with initial moisture content of 0.1 (a) and soil type 11 with initial moisture content of 0.3 (b).

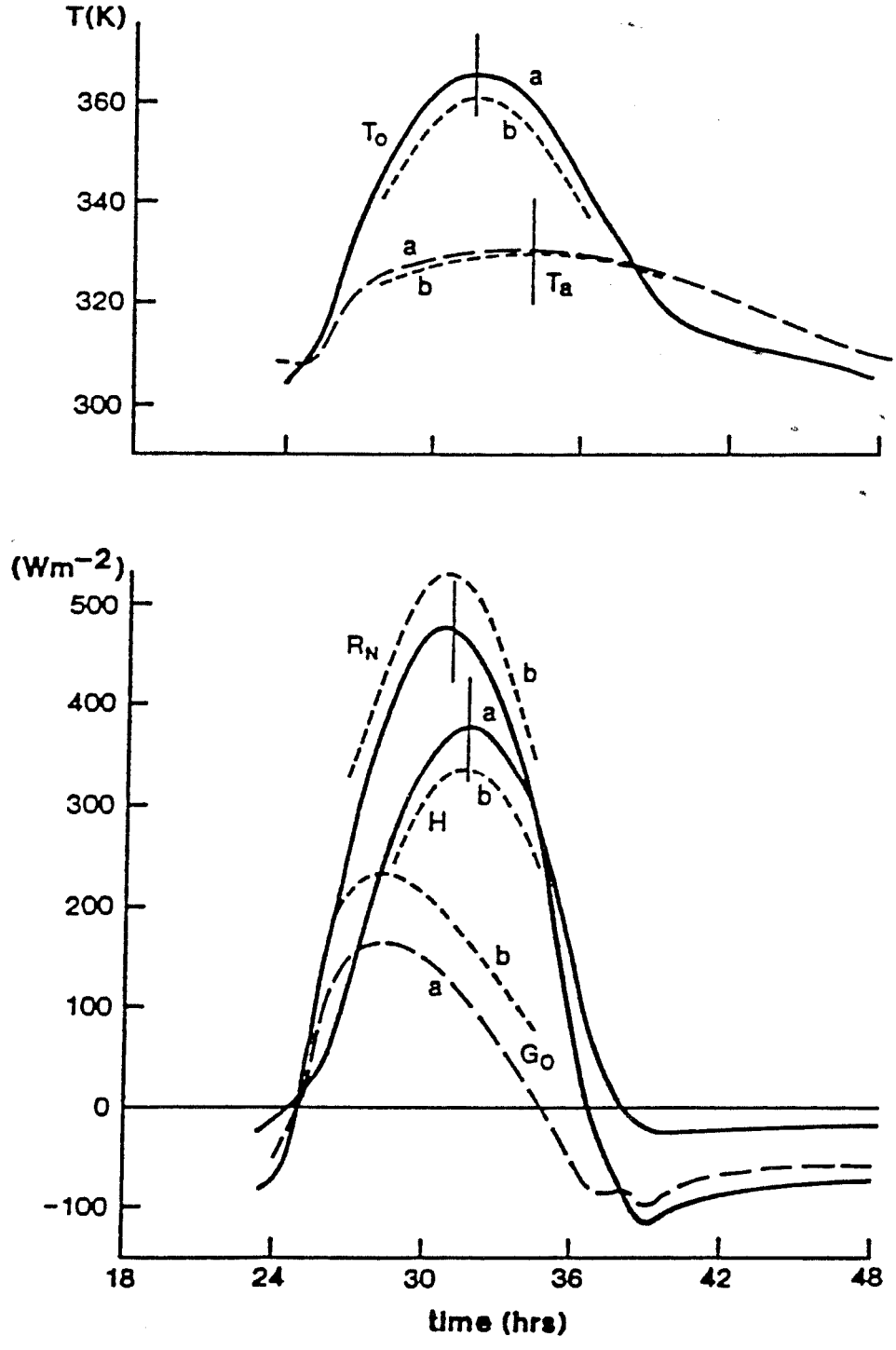

Figure 10: Simulations of the diurnal cycle of surface and air temperatures in extreme conditions, together with components of the surface energy balance equation. Curves are based on simulations using the full 1D mesoscale model with multi-layer soil scheme (curves a) and the 1D stand-alone model (curves b). The time axis is in hours after initialization of the respective models.

TABLE 1: Values of c_g ($c_g = \rho_s c_s d_1'$), the heat capacity per unit area of a range of natural surfaces, with the water depth equivalent W.D.E. (assumes $1cm$ depth of water has $c_g = 4.18 \times 10^4 Jm^{-2}K^{-1}$) and damping depth $d_1' = 2(\kappa_s/2\omega)^{1/2}$.

Material	c_g $(Jm^{-2}K^{-1})$	W.D.E. (mm)	d_1' (cm)
Water	1.3×10^5	31	6
Dry Sand	7.0×10^4	17	8
Wet Clay	2.5×10^5	60	12
New Snow	1.6×10^4	4	7
Air	435	0.1	76
Canopy			
$99.5\%air, 0.5\%H_2O$	1000	0.2	-
$90.0\%air, 10\%H_2O$	1.3×10^4	3	-

5 Canopy parameterization

a) Canopy-soil temperature and moisture, and surface fluxes

The above descriptions are valid for a bare soil surface only; where vegetation is present a simple, but realistic, parameterization scheme is required to represent the effects of vegetation on energy partitioning at the surface, rainfall interception and soil moisture. In such a scheme it is usual to represent the canopy as a single vegetation layer with the characteristics of a large leaf acting as a source or sink of water vapour and sensible heat. The degree to which the canopy shields the ground from the solar radiation is characterised by the parameter σ_f, denoting the fraction of vegetation within a computational grid, and equal to 1 for complete blocking and to 0 for no foliage. Two methods of calculating the surface temperature and hence surface fluxes, are presented here - both are options in the 1D S/A model and in the GCM scheme.

In the first method, an isothermal assumption for the canopy-soil combination allows the use of the 'force-restore' approach (section 4) for calculation of the canopy-soil temperature. The thermal inertia of the canopy-soil layer is expressed as (Noilhan and Planton, 1989):

$$C_T = ((1 - \sigma_f)c_g + \sigma_f c_v)^{-1} \tag{43}$$

where $c_g = \rho_s c_s d_1'$ is the thermal inertia (heat capacity per unit surface area) of the ground, with d_1' given by equation (41), and c_v is the thermal inertia of the vegetation. Usually $c_v \ll c_g$. Table 1 summarises values of c_g for a range of surface types, with c_v values given for vegetation based on simple considerations and values quoted in the literature. Also shown are the equivalent water depths (1 cm of water has $\rho_s c_s = 4.18 \times 10^6 Jm^{-3}K$), and the damping depth d_1'.

The prognostic equation for the temperature of an isothermal near-surface soil/canopy layer (similar to Eq.(39)), is described as follows:

$$\frac{\partial T_{f,g}}{\partial t} = -c_1 C_T H_A - c_2 \frac{T_{f,g} - T_b}{\tau} \tag{44}$$

and the bulk temperature:

$$\frac{\partial T_b}{\partial t} \approx -\frac{H_A}{\rho_s c_s d_2'} \tag{45}$$

where d_2' is given by Eq.(42). H_A is given by the surface energy balance equation:

$$\begin{aligned} H_A = -[&\sigma_f(1-\alpha_f)R_{so}\downarrow + (1-\sigma_f)(1-\alpha_g)R_{so}\downarrow + R_{Lo}^d\downarrow \\ &-(1-\sigma_f)\epsilon_g\sigma T_{f,g}^4 - \sigma_f\epsilon_f\sigma T_{f,g}^4 - (H + \sigma_f\lambda E_f + (1-\sigma_f)\lambda E_g)] \end{aligned} \tag{46}$$

where $R_{so}\downarrow$ is the incoming solar radiation, $R_{Lo}^d\downarrow$ is the incoming long wave radiation, α_f is foliage albedo, α_g is ground albedo, ϵ_g is the emissivity of the ground, ϵ_f is the emissivity of the foliage, σ is the Stefan-Boltzmann constant, H is the sensible heat flux (its components, H_f and H_g, are assumed the same when $T_f = T_g$), and E_f, E_g are the latent heat fluxes of foliage and ground respectively.

A second, preferable, method of computing the surface temperature $T_{f,g}$ and the surface fluxes is to calculate separately the soil (T_g) and canopy (T_f) temperatures. Soil temperature T_g is obtained from Eq.44 where H_A

and C_T are computed from Eqs.46 and 43 with $\sigma_f = 0$. The sensible heat flux $H(=H_g)$ entering Eq.46 is now obtained from

$$H_g = \rho_a c_p \frac{(T_g - T_a)}{r_{aH1}} \tag{47}$$

where r_{aH1} is taken to be the aerodynamic resistance over a bare soil surface. The canopy temperature T_f is obtained from the solution of the surface energy balance equation

$$(1-\alpha_f)R_{so}\downarrow + R^d_{Lo}\downarrow - \epsilon_f \sigma T_f^4 - H_f - \lambda E_f = 0, \tag{48}$$

where the sensible heat flux H_f is given by:

$$H_f = \rho_a c_p \frac{(T_f - T_a)}{r_{aH2}} \tag{49}$$

where r_{aH2} is the aerodynamic resistance over the canopy.

The water vapour flux over an area is assumed to arise from evaporation from the soil surface, E_g, and evaporation from the canopy E_f, itself comprising evaporation from the fraction of canopy covered with water, E_w (i.e. potential evaporation), and transpiration from the remaining part of the dry canopy E_{tr}. Evaporation from the ground is calculated from Eq.(37). Evaporation from the wet canopy is given by:

$$E_w = \rho_w \frac{(q^*(T_f) - q_a)}{r_{aV2}}. \tag{50}$$

where q^* is the saturation specific humidity at the foliage temperature. The resistance r_{aV2} is appropriate to the vegetated fraction of the grid area, and compares with (as used in Eq. 26) r_{aV1} for bare soil. Transpiration is parameterized as:

$$E_{tr} = \rho_w \frac{(q^*(T_f) - q_a)}{r_{aV2} + r_s}. \tag{51}$$

where r_s is the bulk stomatal (surface) resistance. The presence of vegetation increases the evaporation due to extraction, by transpiration, of water from the deep soil.

The soil moisture contents are calculated from a moisture scheme for the combined canopy-soil surface layer, as follows (cf. Eqs. 31,34):

$$\frac{\partial \eta_g}{\partial t} = -C_1 \frac{(1-\sigma_f)E_g - ((1-\sigma_f)P\rho_w + \sigma_f P_g \rho_w + M_s \rho_{snow} - R\rho_w)}{\rho_w d_1} - C_2 \frac{\eta_g - \eta_{eq}}{\tau} \tag{52}$$

while the bulk layer moisture is given by:

$$\frac{\partial \eta_2}{\partial t} = -\frac{\sigma_f(1-\beta)E_{tr}}{\rho_w d_2} + \frac{d_1}{d_2} C_2 \frac{(\eta_g - \eta_{eq})}{\tau} \tag{53}$$

where β is defined by Eq.60. The scheme is an extension of the bare soil formulation (see section 3). Note that evaporation occurs only from the fraction of grid with bare ground while $((1-\sigma_f)P\rho_w + \sigma_f P_g \rho_w + M_s \rho_{snow} - R\rho_w)$ represents the water flux reaching the ground. For a bare ground $P_g = P$, and for a canopy, rain must first fill a reservoir of water on a canopy (m_c), so that:

$$P_g = \begin{cases} 0 & \text{if } m_c < m_{c,max} \\ P & \text{if } m_c = m_{c,max}. \end{cases}$$

The equation for bulk moisture (53) now contains a term describing the moisture uptake through the roots and its transport to the atmosphere through transpiration.

Finally, the combined soil-canopy temperature now is:

$$T_{f,g} = (1-\sigma_f)T_g + \sigma_f T_f, \tag{54}$$

and the combined fluxes are:

$$H_o = (1-\sigma_f)H_g + \sigma_f H_f \tag{55}$$

$$E_o = (1-\sigma_f)E_g + \sigma_f E_f \tag{56}$$

where

$$E_f = (1-\beta)E_{tr} + \beta E_w. \tag{57}$$

(b) Rainwater and dew interception

Rainfall and dew intercepted by the canopy are stored in a reservoir, of water content m_c. The equation for the water content (units of depth) of the reservoir is:

$$\frac{\partial m_c}{\partial t} = P - \beta E_w/\rho_w \tag{58}$$

where P is precipitation above the vegetation. The precipitation at the ground $P_g = P$ when m_c exceeds a critical value $m_{c,max}$ defined by Dickinson, (1984) as:

$$m_{c,max} = 0.2LAI[mm] \tag{59}$$

where $m_{c,max}$ is the maximum depth of the film of water that vegetation can hold. Reported values of $m_{c,max}$ vary between $0.4mm$ for grass to about $2mm$ for trees, Rutter,(1975). LAI varies from 0.3 for sparse canopy to 10 for dense vegetation. E_w is a wet-surface evaporation from the reservoir of water to the atmosphere (i.e. evaporation at zero stomatal resistance) or a dew deposition when the foliage temperature falls below the dew point of the air. β is the fraction of the foliage covered with a film of water, and is set as a function of the depth of the interception reservoir as defined by Deardorff, (1978):

$$\beta = \begin{cases} 1 & \text{if } condensation \\ m_c/m_{c,max} & \text{if } evapotranspiration. \end{cases} \tag{60}$$

Canopy interception is an important process as it allows for immediate evaporation from a wet surface, which is generally much higher than transpiration from the dry canopy surface.

c) Stomatal resistance

Canopy transpiration is controlled by the opening and closing of the plant stomata. This resistance to the diffusion of water vapour out of leaves is called a stomatal resistance. In all of the canopy parameterization schemes the stomatal resistance formulation plays a central role. The resistance depends on a range of factors including atmospheric conditions, availability of soil moisture, and vegetation type (e.g. Gates, 1980, chap. 10). The formulation used in the 1D S/A model is based on Noilhan and Planton (1989), viz.

$$r_s = \frac{r_{si}^+}{LAI} F_1 F_2^{-1} F_3^{-1} F_4^{-1} \tag{61}$$

where $r_s^+ = r_{si}^+/LAI$ is an unconstrained canopy (stomatal) resistance and is dependent on vegetation type and LAI. Table 2 shows examples of r_s^+ and the minimum observed (day time) values of r_s, $[r_s(min)]$. In the above, F_1 parameterizes the effect of the photosynthetically active radiation

$$F_1 = \frac{1+f}{f + r_{si}^+/5000} \tag{62}$$

TABLE 2: Values of the unconstrained canopy (stomatal) resistance r_s^+ at a specified LAI and minimum daytime resistance $r_s(min)$ for a range of full canopies.

Canopy Type	Reference	r_s^+ (sm^{-1})	$r_s(min)$ (sm^{-1})
Tropical Forest	Dorman and Sellers, 1989	50	
	Shuttleworth et al. 1984a		125-150
	Shuttleworth, 1989	43	80
Deciduous	Dorman and Sellers, 1989	50	
	Verma et al. 1986		75-160
	Shuttleworth, 1989	41	70-100
Coniferous	Dorman and Sellers, 1989	60	
	Jarvis et al. 1976		90-150
	Noilhan and Planton, 1989	43	
	Shuttleworth, 1989	56	70-100
Savannah	Garratt, 1978		100
Grassland	Dorman and Sellers, 1989	40	
	Russell, 1980		40
Crops	Dorman and Sellers, 1989	30	30-35
	Sellers and Dorman, 1987	20-75	
	Perrier, 1982		40-130
Maize/Oats	Noilhan and Planton, 1989	20-150	

with

$$f = 0.55 \frac{S\downarrow}{S^*} \frac{2}{LAI} \tag{63}$$

where $S\downarrow$ is an incoming solar radiation, S^* is a limit value of $30 Wm^{-2}$ for a forest and $100 Wm^{-2}$ for a crop. F_2 describes availability of the water in the root zone for transpiration:

$$F_2 = \begin{cases} 1 & \text{if } \eta_2 > 0.75\eta_{sat} \\ (\eta_2 - \eta_{wilt})/(0.75\eta_{sat} - \eta_{wilt}) & \text{if } \eta_{wilt} \leq \eta_2 \leq 0.75\eta_{sat} \\ 0 & \text{if } \eta_2 < \eta_{wilt}. \end{cases} \tag{64}$$

For a soil water content below the wilting moisture content, transpiration

from the vegetation becomes zero. The value of η_{wilt} decreases from 0.286 for clay, to 0.175 for sandy clay loam, and 0.068 for sand.

The function F_3 represents the effect of vapour pressure deficit in the air, and takes the form (e.g. as proposed by Jarvis et al. 1976):

$$F_3 = 1 - g(e^*(T_{f,g}) - e_a) \tag{65}$$

where g is an empirical parameter, $e^*(T_{f,g})$ is the saturated vapour pressure at temperature $T_{f,g}$ and e_a is the vapour pressure at temperature T_a. The function F_4 allows for a temperature dependence of the stomatal resistance with increasing value at high or low temperatures, with:

$$F_4 = 1.0 - 0.0016(298.0 - T_a)^2. \tag{66}$$

d) Validation tests

The canopy parameterization in the 1D S/A model is based on the theory of air-surface exchange over locally homogoneous surfaces. Therefore, we attempt to validate the scheme against single station experimental data. The list of parameters and quantities required for soil and vegetation description is as follows:

Soil

η_{sat} - saturated moisture content
η_{wilt} - wilting moisture content
ψ_{sat} - saturation value of matrix potential
c_s - specific heat
ρ_s - density
α_g - albedo
ϵ_g - emissivity

Vegetation

r_s^+ - minimum observed canopy (stomatal) resistance (unconstrained)
σ_f - fraction of vegetation
LAI - leaf area index
z_0 - roughness length
α_f - albedo
ϵ_f - emissivity

TABLE 3: Representative values of the specific heat c_s, density ρ_s, thermal conductivity k_s, thermal diffusivity κ_s, longwave emissivity ϵ_g for two soil types and snow. Also, for soils, saturation moisture η_{sat}, wilting moisture η_{wilt} and saturated matrix potential ψ_{sat}.

Surface	η_{sat}	η_{wilt}	ψ_{sat} m	c_s $Jkg^{-1}K^{-1}$	ρ_s kgm^{-3}	k_s $Wm^{-1}K^{-1}$	κ_s m^2s^{-1}	ϵ_g
Clay Soil	0.48	0.29	-0.40					
dry				890	1600	0.25	0.18	0.95
wet				1550	2000	1.58	0.51	0.97
Sand Soil	0.39	0.07	-0.12					
dry				800	1600	0.3	0.24	0.95
wet				1480	2000	2.2	0.74	0.98
Snow								
new				2090	150	0.1	0.3	0.95
old				2090	640	1.0	0.7	0.90

TABLE 4: Data from the Hapex-Mobilhy experiment (Noilhan and Planton, 1989).

Site	Veget.	η_g m^3m^{-3}	η_2 m^3m^{-3}	z_0 m	α_s	LAI m^2m^{-2}	r_{si}^+ sm^{-1}	σ_f
Estampon	Forest	0.14	0.20	1.0	0.10	2.3	100	0.99
Lubbon 1	Oats	0.10	0.14	0.15	0.21	3.0	450	0.90
Lubbon 2	Maize	0.17	0.17	0.1	0.15	2.0	40	0.80

For a selected soil type, parameters such as η_{sat}, η_{wilt}, ψ_{sat}, c_s, ρ_s, k_s, κ_s, ϵ_g are summarised in Table 3. For vegetation, much of the required information has been inferred from observations.

Four data sets have been used for validation purpose - three from the Hapex-Mobilhy experiment (Noilhan and Planton, 1989) and one for the Amazon forest described in Sato et al. (1989). Table 4 summarizes data for three surfaces in the Hapex-Mobilhy experiment.

All of these data, except r_s^+, were used in the 1D S/A model simulations. The initial temperature and humidity profiles were derived from mean climatological data for the given geographical position and time of the year. r_s^+ values were adjusted to reproduce the observed heat fluxes, and compared with literature (and other derived) values.

Fig.11a shows the daily variation of the simulated latent, sensible and soil heat fluxes in comparison with observations for a forest area. Vegetation completely covers the ground ($\sigma_f = 0.99$) giving negligible soil heat flux. Quite good agreement for sensible heat flux is obtained. The simulated latent heat flux reaches the same maximum value of about $300 Wm^{-2}$, but is slightly higher in the afternoon. The optimum value of $r_{si}^+ = 140 sm^{-1}$ is greater than the value given in Table 4. Shown in Fig. (11 b) is the simulated diurnal variation of air temperature , looking quite realistic, but for which there are no observations for comparison.

The second case describes a field of mature oats, Fig. (11 c,d). Observed evaporation is very low due to low soil moisture and the maturity of the plants. The simulated latent heat flux agrees very well with observations, except in the evening hours when it is overestimated. The sensible heat flux is well reproduced. Simulated air temperatures (Fig 11d) are in excellent agreement with observations. The optimum value of $r_{si}^+ = 450 sm^{-1}$ is the same as in Table 4.

The last of the Hapex-Mobilhy data corresponds to a field of maize, Fig. (11 e,f). The simulated latent heat flux agrees well with observations, and the sensible heat flux is slightly underestimated in the morning and overestimated during afternoon hours. Stomatal resistance (r_{si}^+) used is higher than that in Table 4, $57 sm^{-1}$ vs $40 sm^{-1}$. Simulated air temperatures through much of the day and night are about 3K lower than observed, Fig. (11f).

We next compare the results (Fig. 11 g,h) of a simulation for the Amazon Basin rain forest. Available observations from Sato et al. (1989) are for 30-day averages. To account for cloudiness (the 1D S/A model does not have a cloud scheme), the daytime shortwave fluxes were decreased and the nighttime atmospheric longwave fluxes increased to reproduce the daytime and nighttime values of net radiation. The maximum values of fluxes observed and predicted, are about $400 Wm^{-2}$ for the latent heat flux and $180 Wm^{-2}$ for the sensible heat flux, though during the morning the observed latent heat flux is lower than that simulated, and in the evening observed sensible heat flux is higher than the simulated values. The value of LAI=7, and the optimum value of $r_{si}^{+} = 280 sm^{-1}$ is used to reproduce the fluxes in Fig. (11 g). The model results compare very well with simulations by Sato et al. (1989) using the Simple Biospheric Model of Sellers et al. (1986). Observed and simulated air temperatures (Fig. 11 h) show good correspondence during the day only.

Overall, the above results indicate that the model can realistically reproduce the partitioning of the available energy at a vegetated surface.

(e) Sensitivity tests

In practice, the evaluation of the sensible and latent heat fluxes is sensitive primarily to the choice of r_s value - this is where the greatest uncertainty lies. The evaluation is less sensitive to the choice of z_o value (hence r_a). We have performed a number of two-day simulations for two of the canopy surfaces, varying in a realistic way values of the critical surface parameter r_s. Figure 12 shows the impact of varying r_s^{+} upon the calculated diurnal variations of turbulent fluxes and air temperature above the two forested surfaces. In the case of the French forest, the standard simulation (r_{si}^{+} equals $140 sm^{-1}$) is compared with simulations having r_{si}^{+} of 100 and $180 sm^{-1}$. For the Amazon forest, the standard simulation (r_{si}^{+} equals $280 sm^{-1}$) is compared with simulations having r_{si}^{+} of 180 and $380 sm^{-1}$.

6 Rainfall and snowfall simulation

Part of the rainfall deposited on vegetation is evaporated directly, while rainfall deposited on the ground can infiltrate the soil. Soil moisture may be evaporated from the surface, particularly if there is no vegetation, or may be lost through transpiration processes. When the precipitation

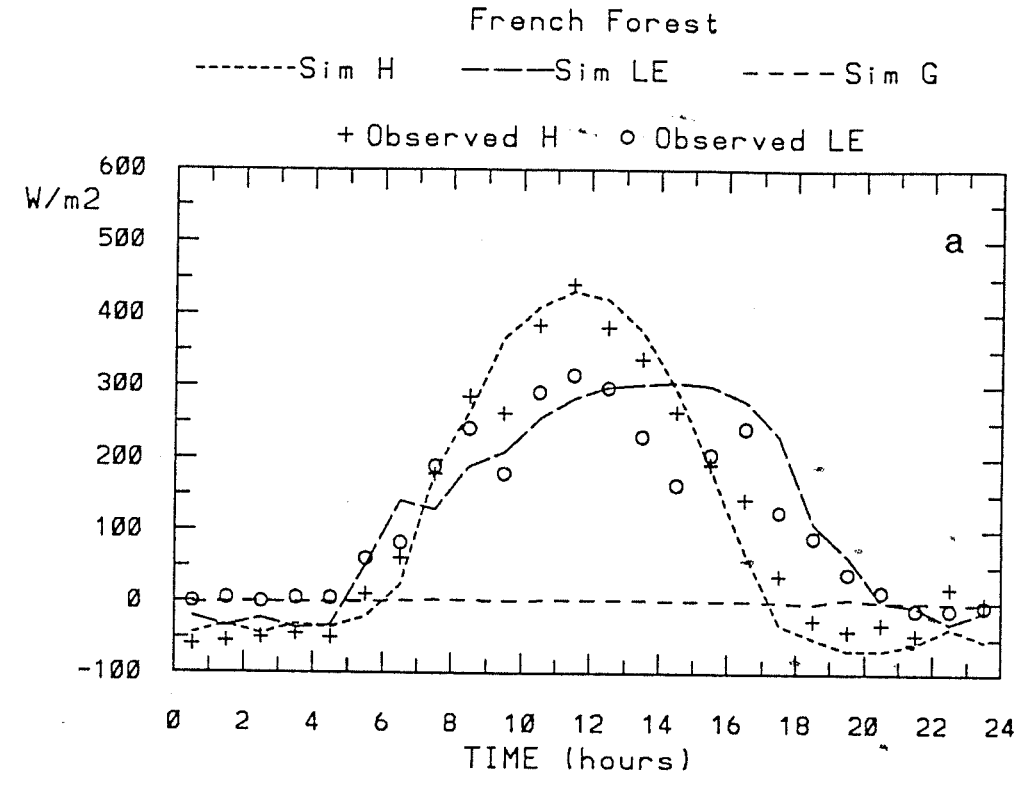

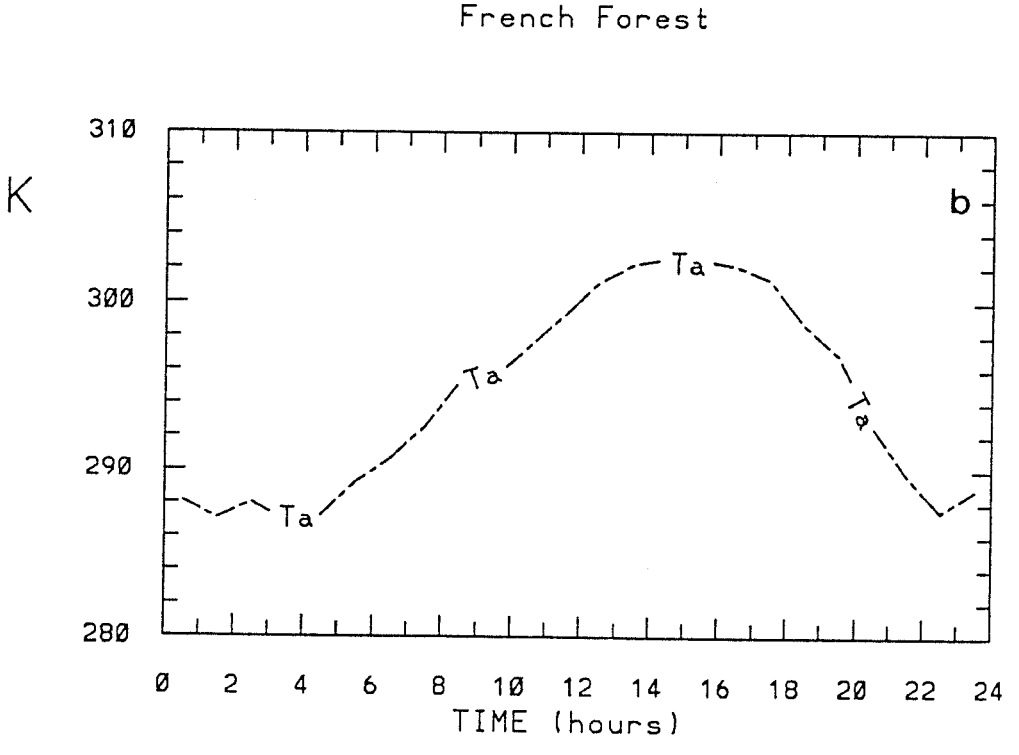

Figure 11(a & b): Comparison of 1D stand-alone model simulations with observations for a temperate forest (HAPEX data), showing diurnal sensible and latent heat fluxes, and ground heat flux (in a) and air temperature (simulation only, in b).

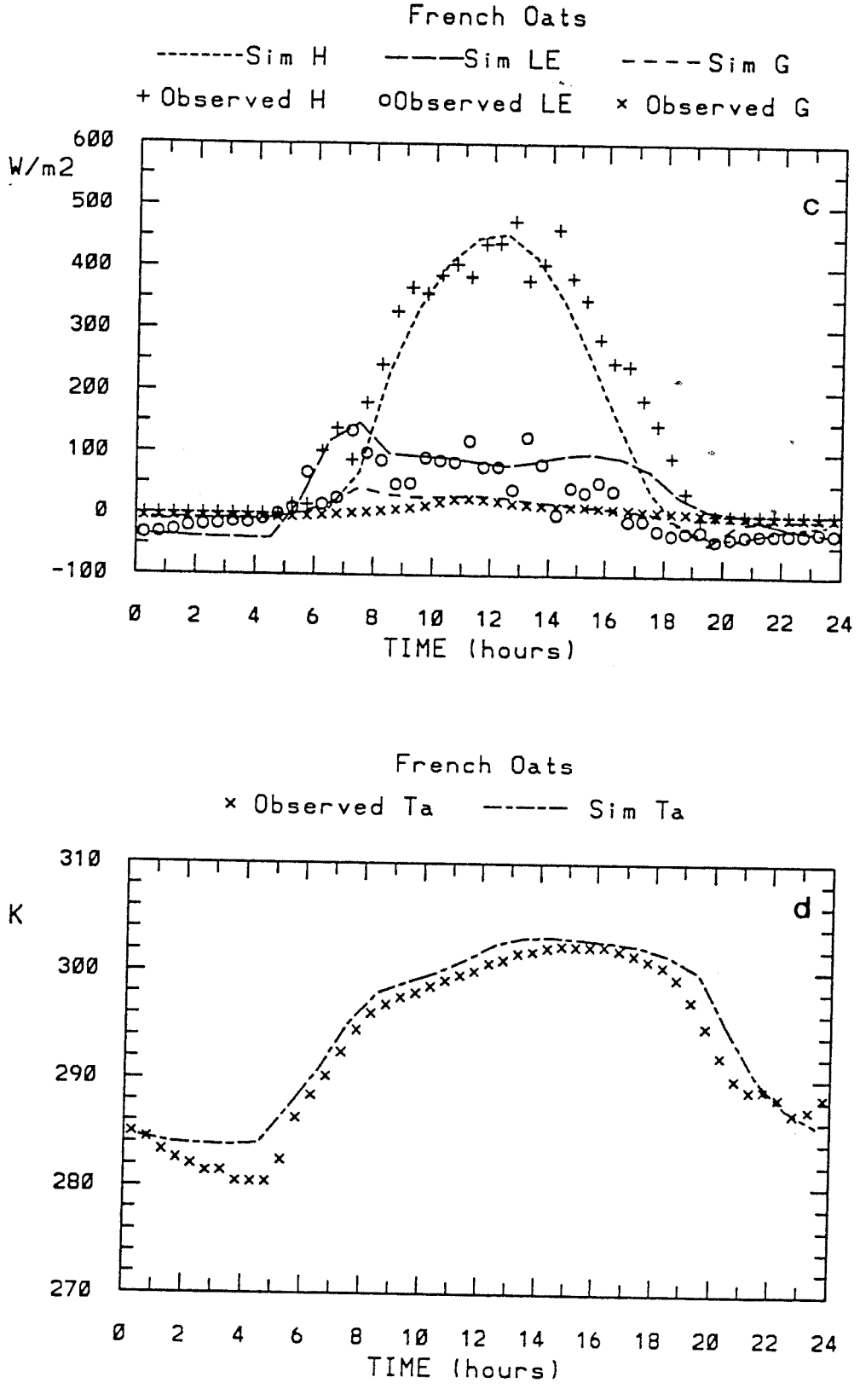

Figure 11(c & d): As in (a & b), for a temperate crop of oats (HAPEX data).

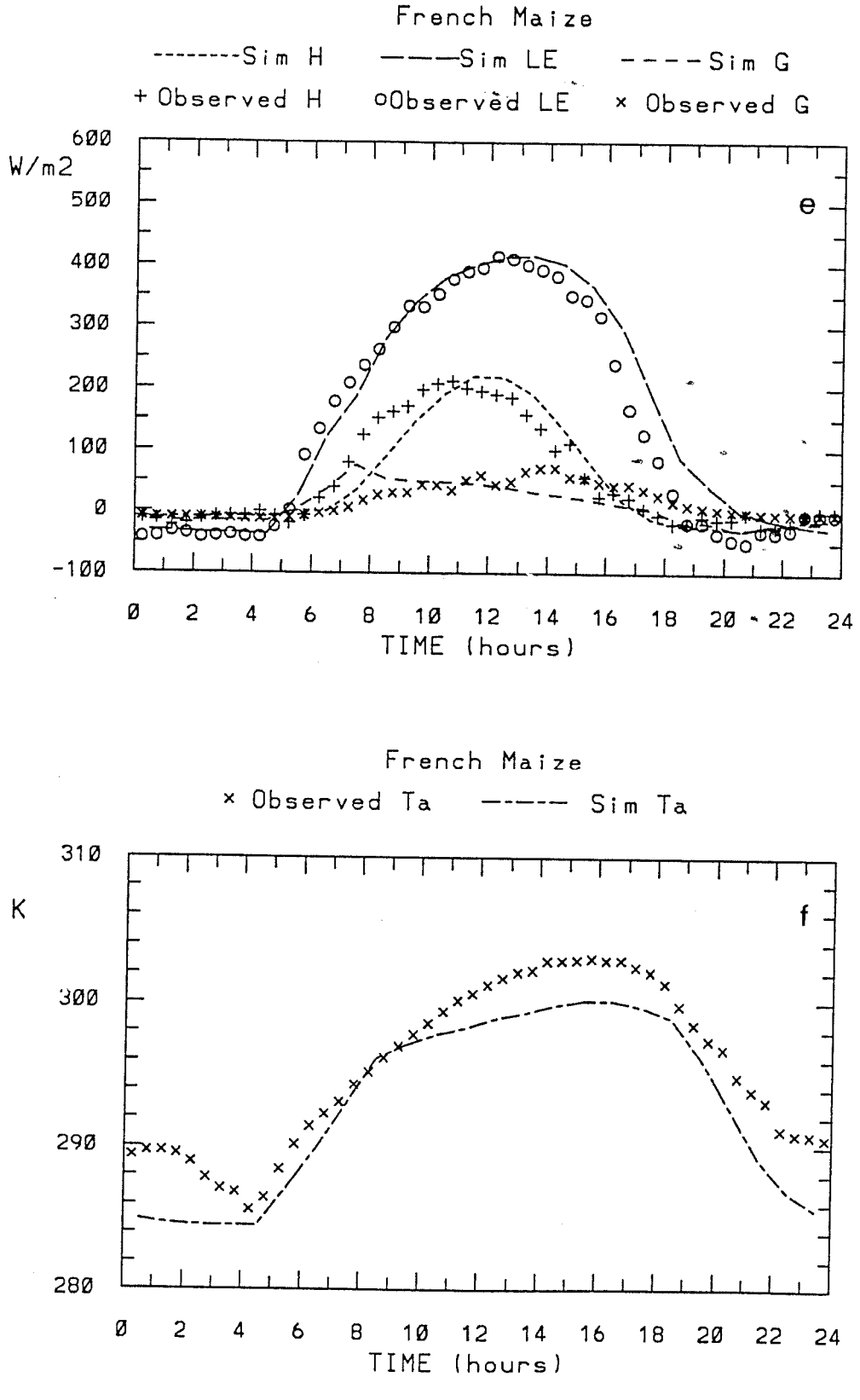

Figure 11(e & f): As in (c & d), for a temperate crop of maize (HAPEX data).

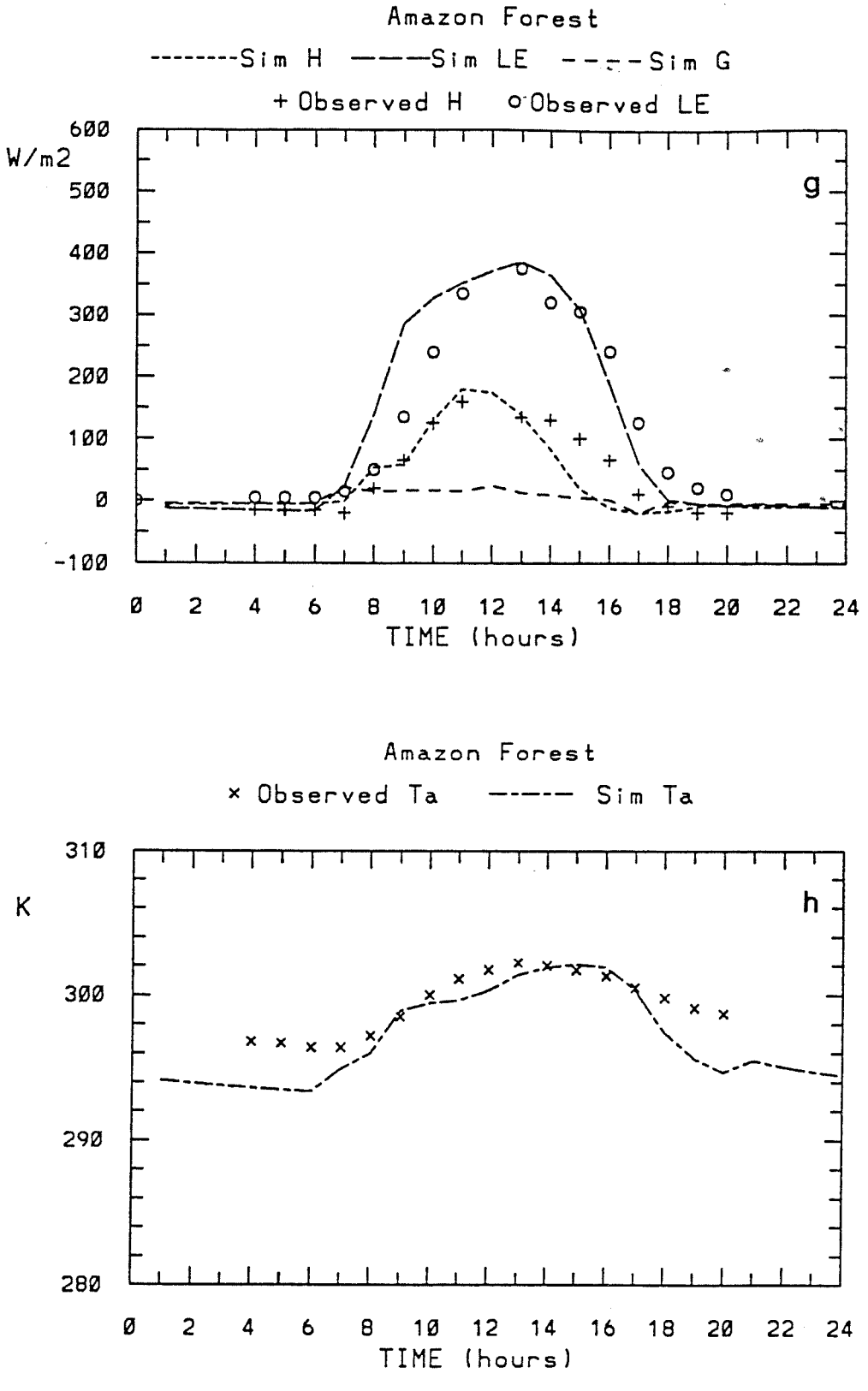

Figure 11(g & h): As in (a & b), for the Amazon forest.

rate exceeds the maximum infiltration rate of the ground, excess water is accumulated as surface runoff. The above processes are represented by Eq. 52, which serves as a budget equation for the moisture content of a layer of soil, which is included in the 1D S/A model. Some account may need to be made of deep-soil percolation.

To demonstrate the performance of the moisture scheme, a 1 day simulation of the soil moisture content in the absence of vegetation, and with a heavy precipitation event, is shown in Fig. (13). Precipitation of $1.75mm/hr$ started 8hr before sunrise and lasted for 8h, see Fig. (13a). The near-surface soil moisture content increased to a saturation value of 0.42 in 6 hours, Fig. (13b). As soon as the surface moisture reached the maximum, infiltration is stopped and surface runoff occurs, Fig. (13c).

In the second simulation, a canopy is present with $r_s^+ = 54s/m$. Precipitation at a rate of $0.4mm/hr$ commences 6 hours before sunrise, and persists for 6 hours, Fig. (14a). Water accumulated on the vegetation reaches its storage capacity of $0.46mm$ after about 1.5 hour of rainfall, Fig. (14b), and remains at this maximum until the cessation of rain ($t = 8hr$). With maximum water on the canopy, precipitation reaches the soil and the soil moisture increases (between $t = 3$ to $8hr$), see Fig. (14c). After cessation of rainfall, water on the canopy evaporates completely within a period of about 3 hours. The greater rate of evaporation from the wet canopy compared with a dry canopy is illustrated on Fig. (14d), showing evaporation rates for 2 simulations, with and without precipitation. The differences in the evaporation rates between $t = 8$ to $10.5hr$ reflect the daytime potential evaporation from the wet canopy; beyond $t = 11hr$, the canopy is dry, Fig. (14b).

In cold climates, in middle to high latitudes in winter, snow covers the ground or vegetation, at least for part of the time. The transpiration by vegetation becomes negligible and in the presence of snow, up to 80% of the incoming solar radiation may be reflected, with considerable reduction (compared with a bare ground) in the heat exchange between the air and surface. This has an impact upon atmospheric dynamics, and upon the water balance. In GCMs, it is important to predict the period of snowcover, the depth of the snow and the snowmelt. Snow or ice loses its mass through sublimation or melting, on a time scale of a few days to months. Melting usually occurs in spring time with the soil surface becoming saturated, with further snowmelt occuring as runoff into rivers and water basins.

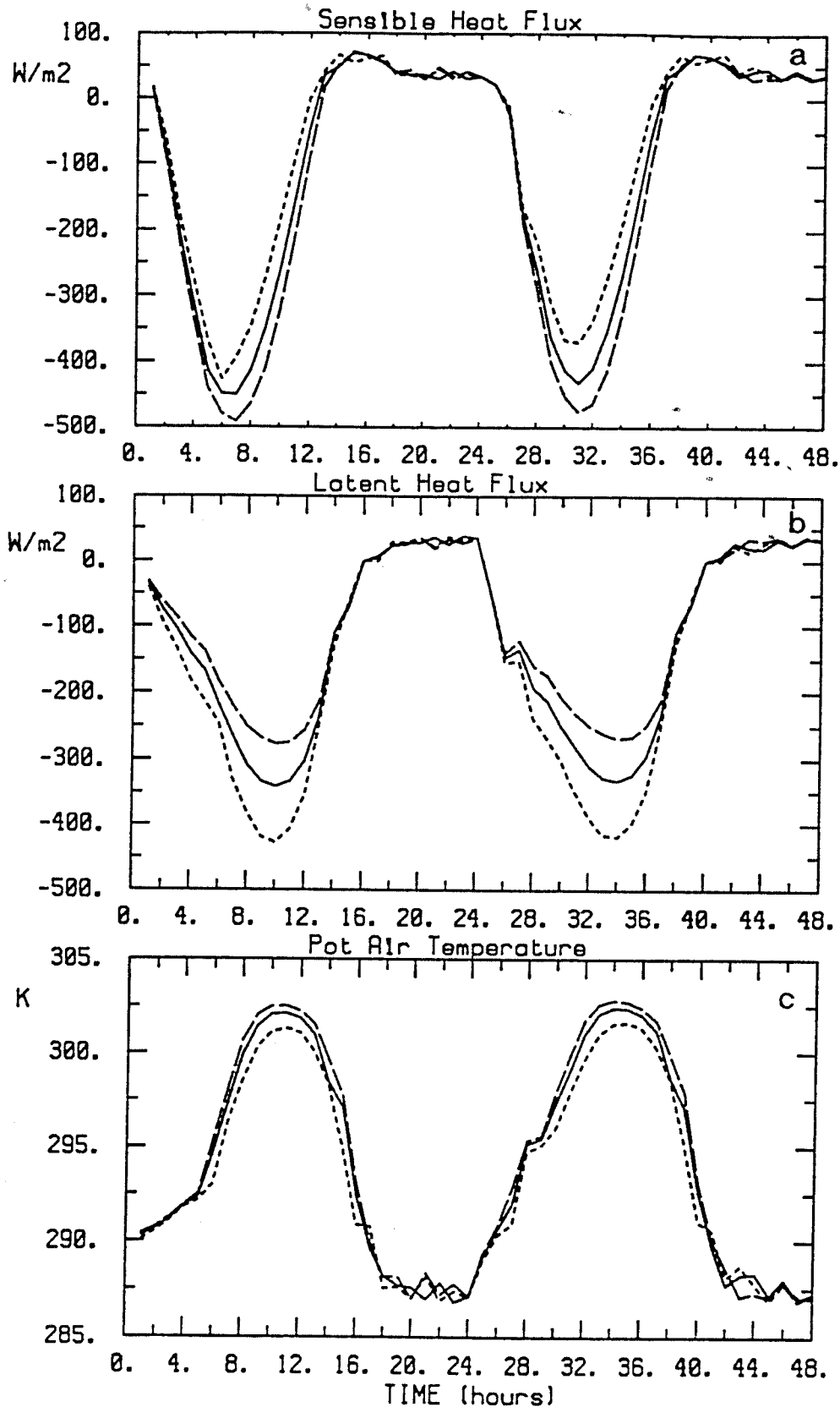

Figure 12(a,b &c): Two-day simulations for two forested surfaces illustrating the sensitivity of the diurnal cycles of sensible and latent heat fluxes, and air temperature, to specified unconstrained surface resistance, r_s^+. Results for the HAPEX forest are shown in (a), (b) and (c), for $r_{si}^+ = 140 sm^{-1}$ (continuous curve), $100 sm^{-1}$ (short pecked curve) and $180 sm^{-1}$ (long pecked curve).

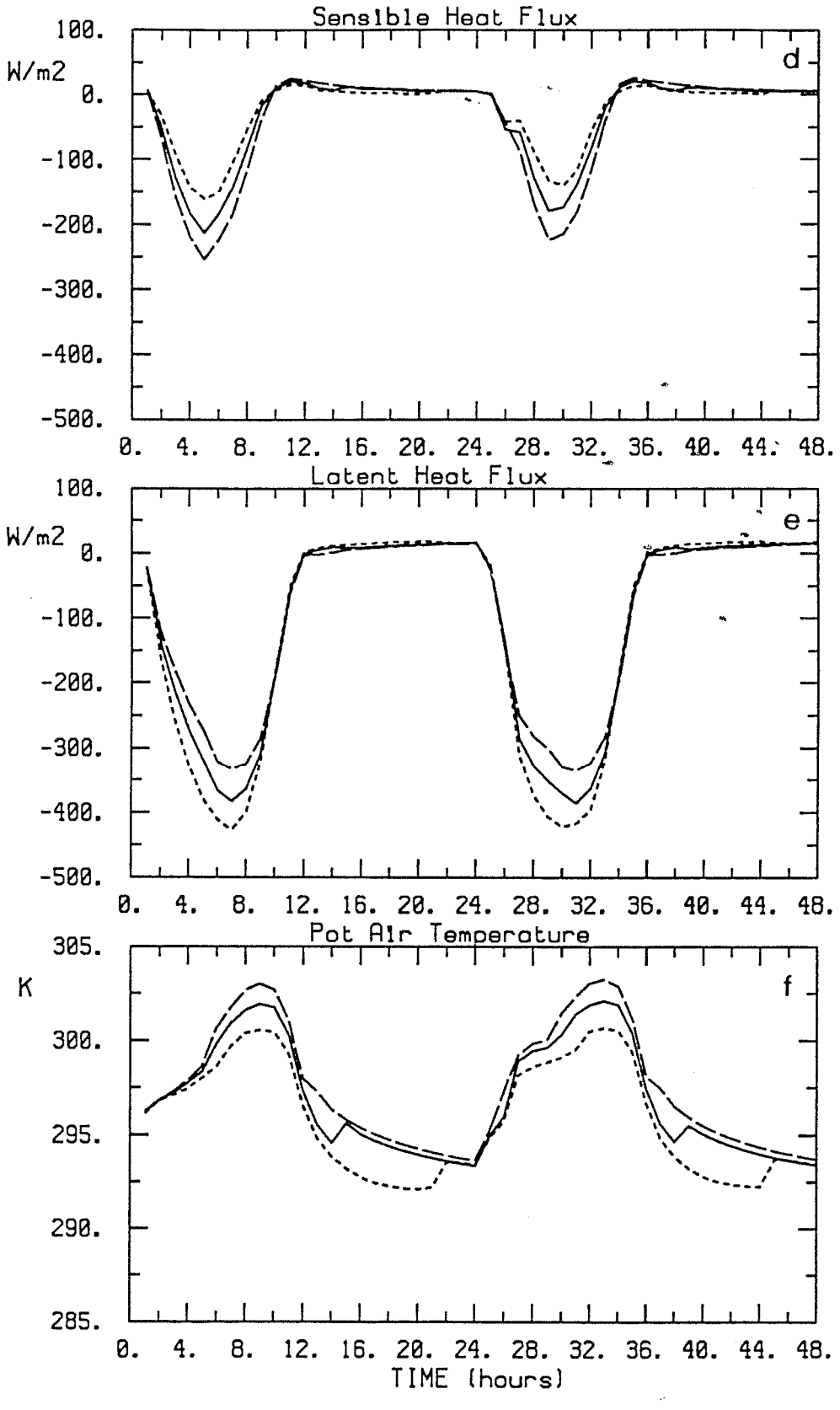

Figure 12(d,e &f): As in 12(a,b &c). Results for the Amazon forest are shown in (d), (e), and (f), for $r_{si}^{+} = 280sm^{-1}$ (continuous), $180sm^{-1}$ (short pecked) and $380sm^{-1}$ (long pecked).

a

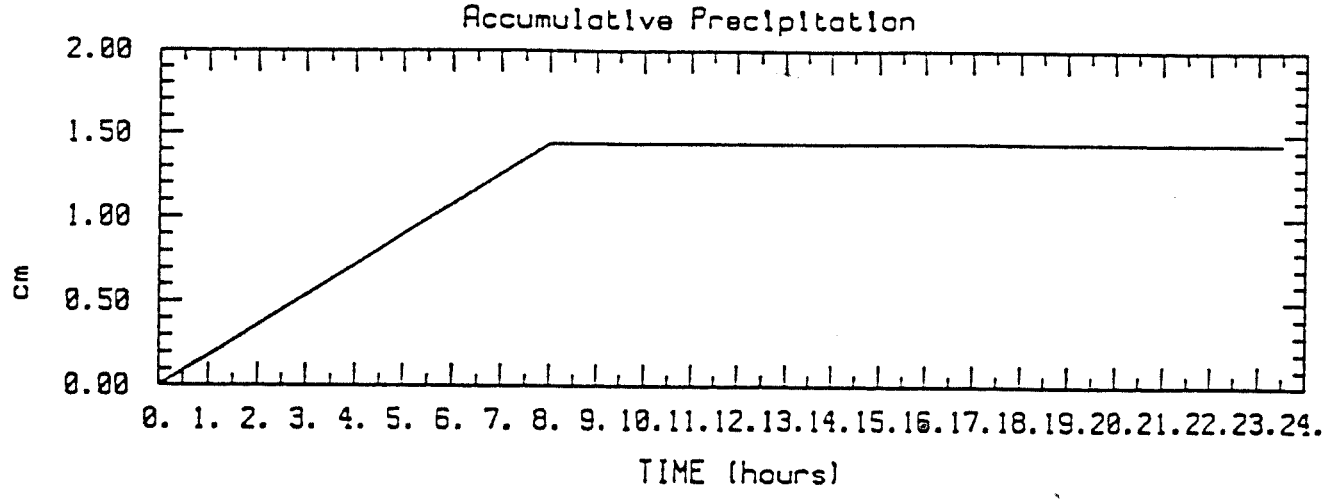

b

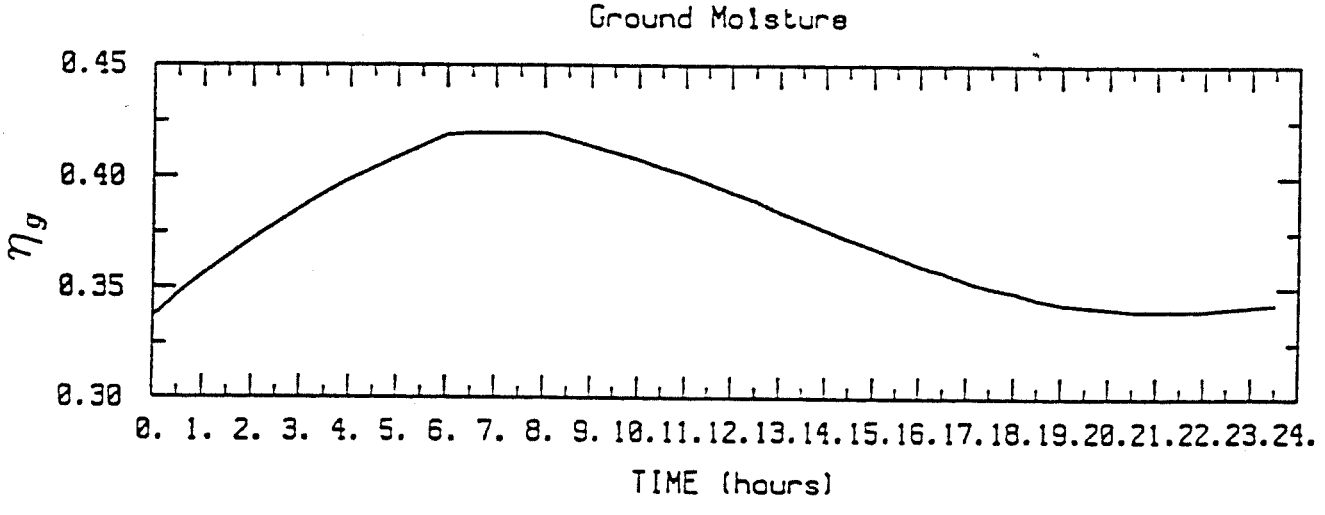

c

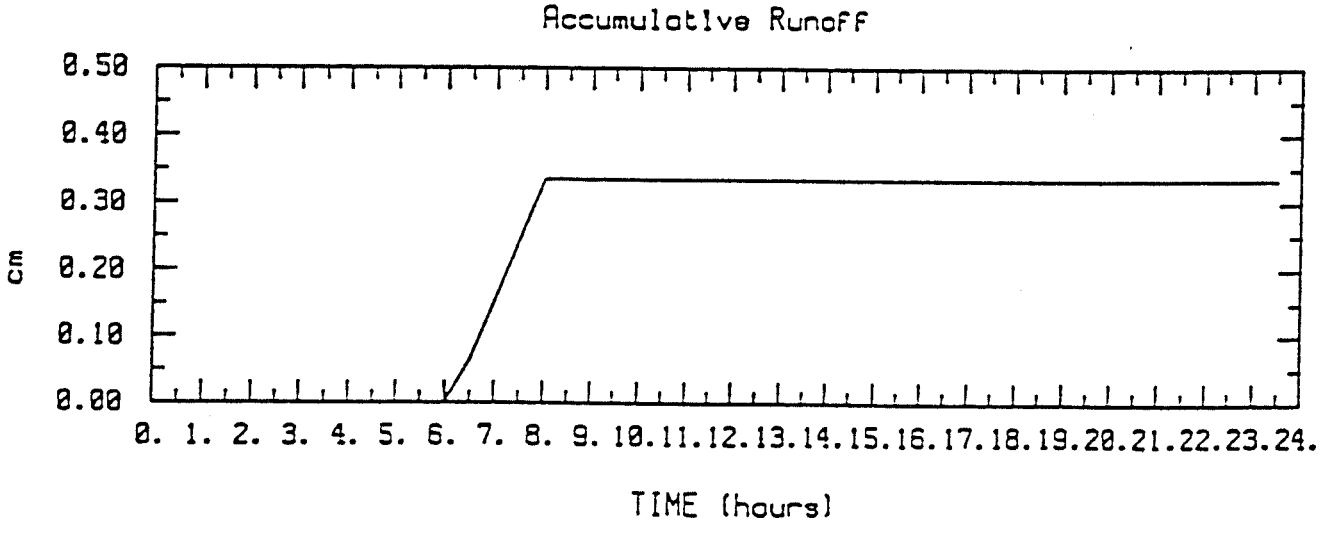

Figure 13(a,b&c): 1D stand-alone model simulation of a rainfall event over bare soil, showing accumulative rainfall (a), ground moisture variations (b) and accumulative runoff (c).

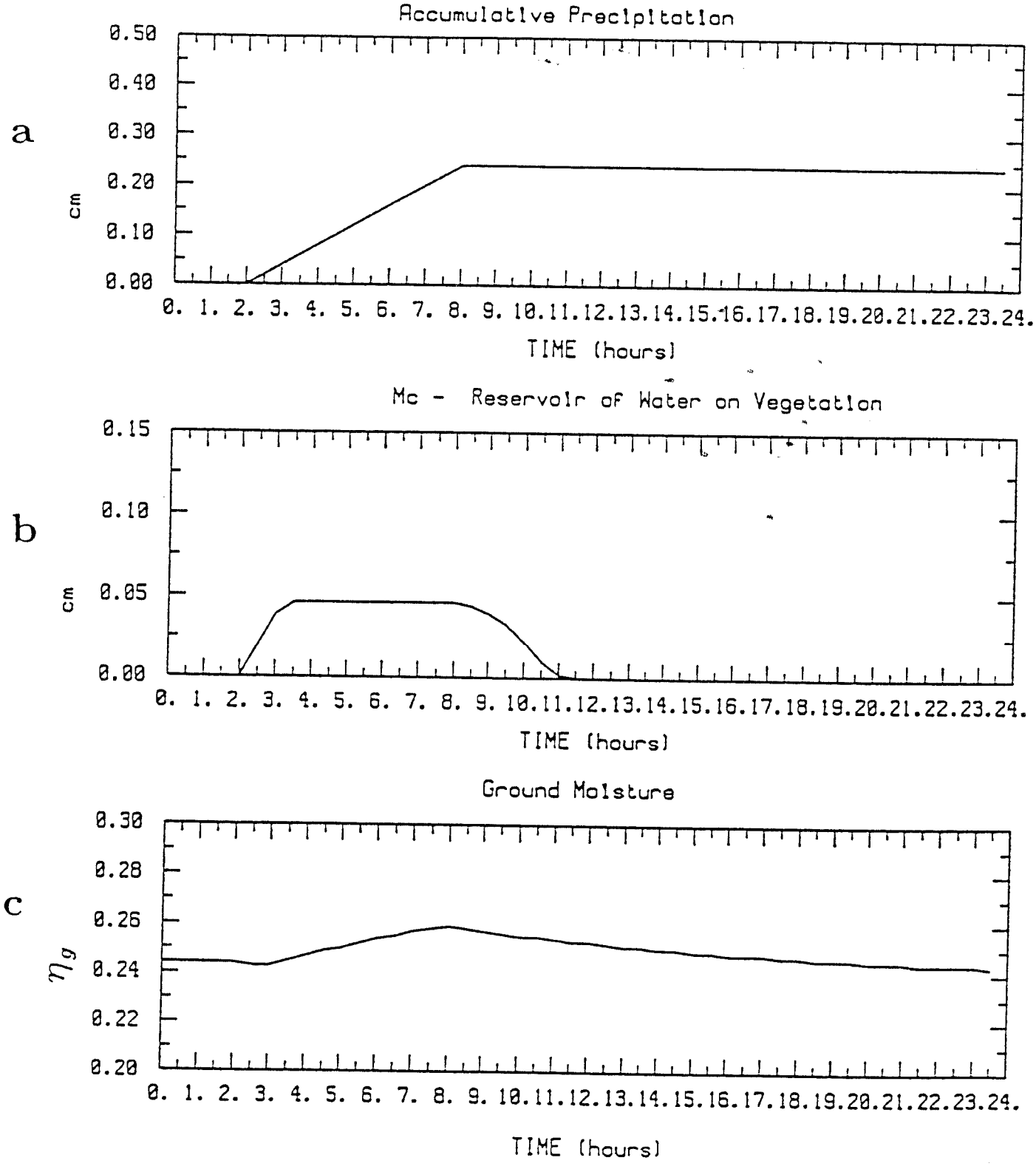

Figure 14(a,b&c): 1D stand-alone model simulation of a rainfall event over a canopy, showing accumulative rainfall (a), variations in the water intercepted by the canopy (b) and ground moisture variations (c).

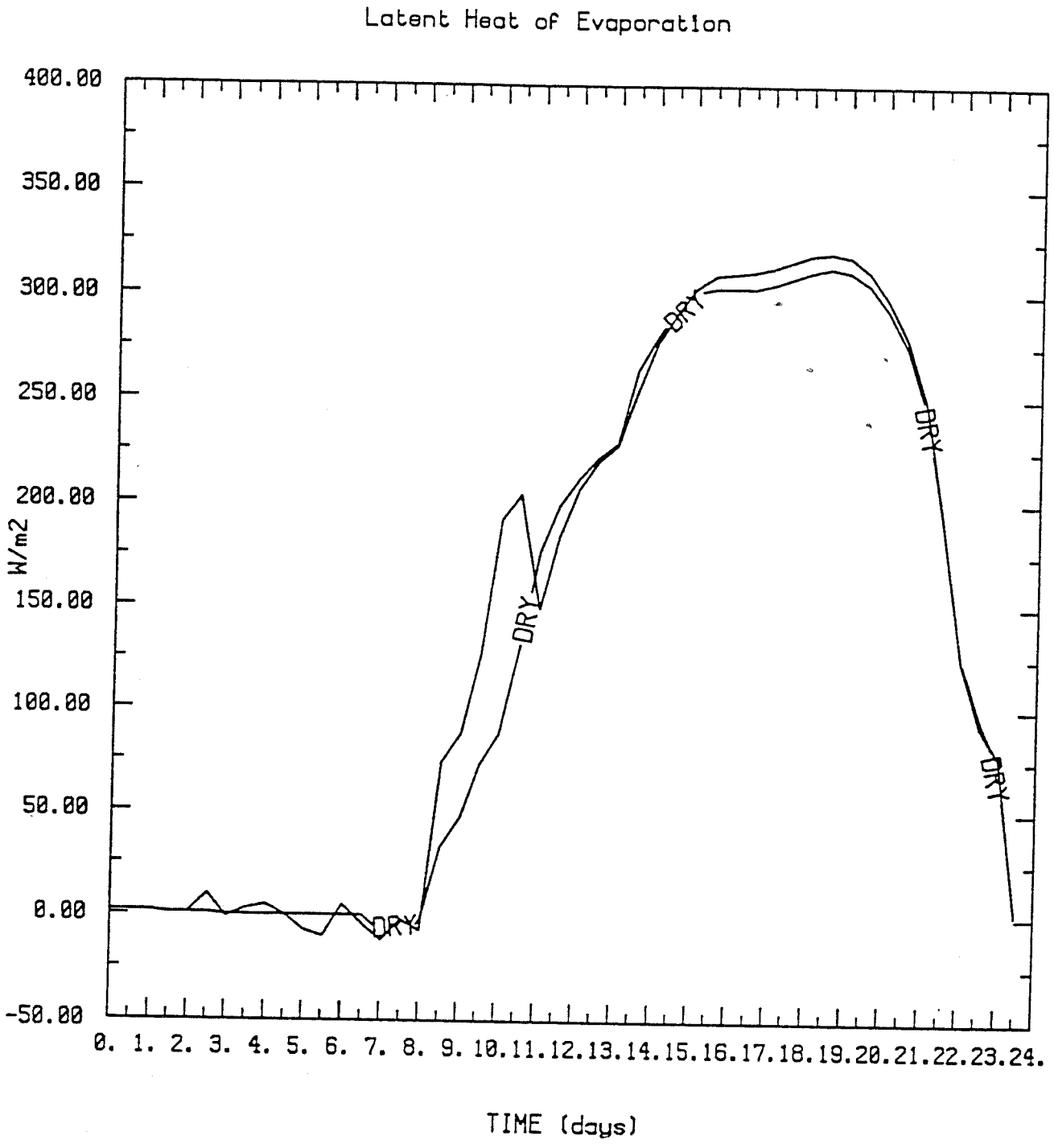

Figure 14(d): 1D stand-alone model simulation of a rainfall event over a canopy, showing the variations in evaporation rates from two simulations with and without precipitation.

In the 1D S/A model, the albedo is made to depend upon snow depth:

$$\alpha = \alpha_{b,g} + (\alpha_{snow} - \alpha_{b,g})\frac{S_n}{S_n + S_n^*} \tag{67}$$

with $\alpha_{snow} = 0.8$ being snow albedo, $\alpha_{b,g}$ is a background albedo, S_n is snow depth and $S_n^* = 1cm$ is a critical snow depth. The evolution of the snow depth (in equivalent water depth) is described as follows:

$$\frac{\partial S_n}{\partial t} = P_s + E_s/\rho_w - M_s/\rho_{snow} \tag{68}$$

where P_s is the precipitation rate, E_s is the sublimation rate or condensation rate (frost) upon the snow, M_s is the rate of snowmelt, and ρ_{snow} is snow density.

To calculate a surface temperature, Eqs. 39 and 41 are used with the volumetric heat capacity ($\rho_s c_s$) and scaling depth d_1' now representing the snow/soil layer. The scaling depth of a deep snow layer is calculated from Eq.41 with κ_s appropriate for snow. If the actual snow depth is smaller than $d_{1,snow}$, the scaling depth and the volumetric heat capacity are made functions of snow depth, i.e. we assume a simple linear combination of the individual soil and snow parameters, so that:

$$d_1' = d_{1,soil}(1 - \frac{S_n}{d_{1,snow}}) + d_{1,snow}\frac{S_n}{d_{1,snow}} \tag{69}$$

$$\rho c = \rho_{soil} c_{soil}(1 - \frac{S_n}{d_{1,snow}}) + \rho_{snow} c_{snow}\frac{S_n}{d_{1,snow}} \tag{70}$$

When the surface temperature is above freezing, melting occurs and the amount of snowmelt (water produced) is calculated from (cf. Eq. 39):

$$M_s = c_1^{-1}\rho_{snow} c_{snow} d_{1,snow}(T_g - 273.16)/(\delta t L_f) \tag{71}$$

with $c_1 = 3.72$, δt is the time step and L_f is the latent heat of fusion. Surface temperature is then reset to 273.16K and the amount of snowmelt (water equivalent) is used in Eq. 68 to calculate a new snow depth and in Eq. 52 to compute the change in soil moisture content.

The results of the simulation of snowfall, and resulting snow accumulation and its impact on albedo and soil moisture, is presented in Fig (15). Snow precipitation ($2cm/hr$ or $2mm/hr$ water equivalent) starts at sunrise and finishes after 6 hours, Fig. (15a).

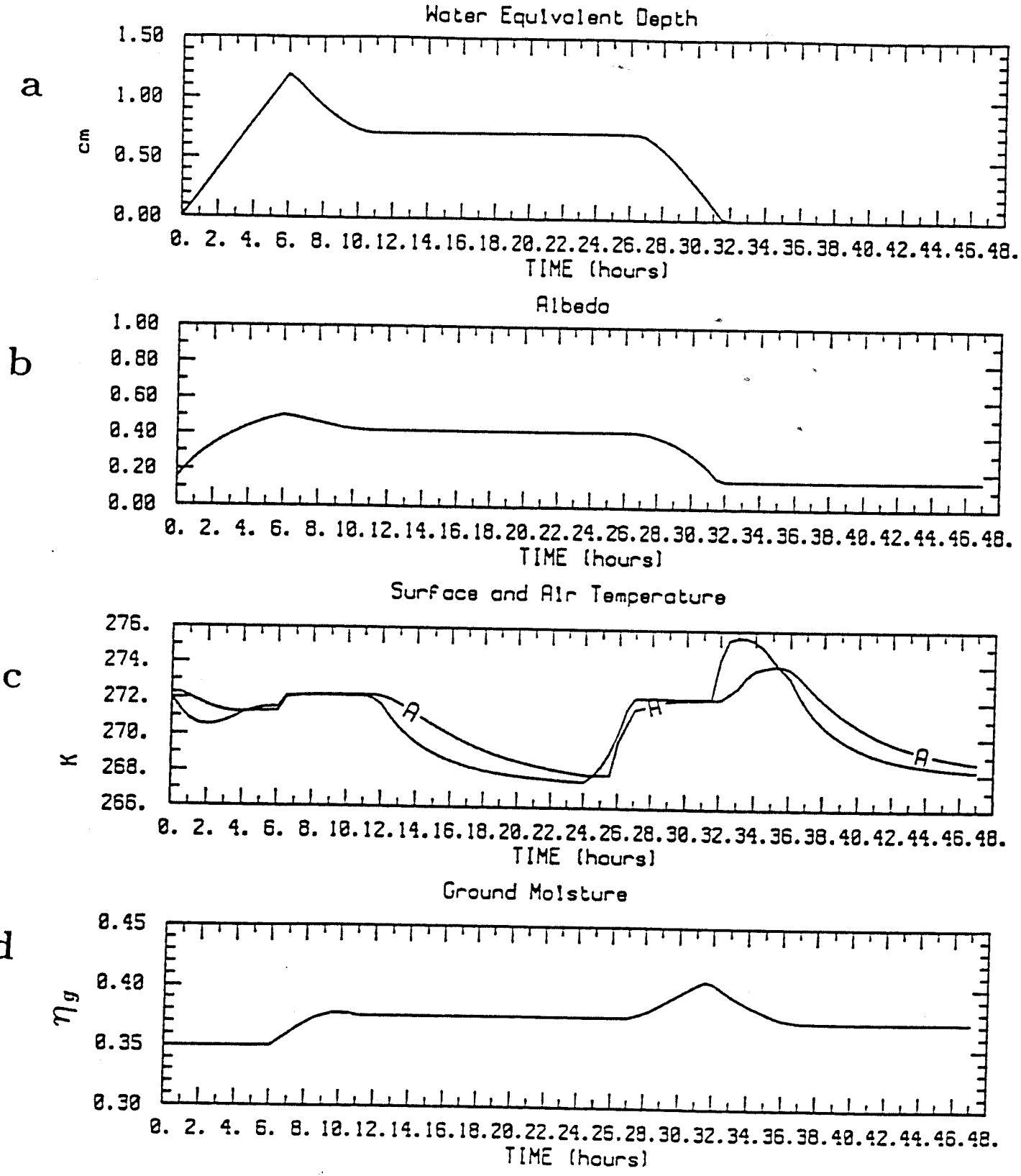

Figure 15: 1D stand-alone model simulation of a snowfall event over bare soil, showing snow depth (water equivalent) (a), snow/surface albedo (b), variations in the surface and air temperatures (c) and ground moisture variations (d).

At 6 hours, the albedo of the surface has changed from 0.15 to 0.5, Fig. (15b), and the accumulated snow depth is $1.2cm$ (in equivalent water depth). Snowmelting starts at hour 6 with the surface temperature rising slightly above freezing, Fig. (15c), and after $4.5hr$ of melting the snow depth is depleted to $0.7cm$ with soil moisture having increased from 0.35 to 0.38, Fig. (15d). Through the night, the temperature remains below freezing and snowmelting resumes 3h after sunrise when the surface temperature rises above freezing. The remaining snow is melted within $4.5hr$, giving rise to a soil moisture content of 0.4.

7 Final Comments

We have described a 1D Stand-alone soil-canopy model that forms the basis of a scheme being incorporated into the 4 and 9 level CSIRO GCMs, for both low and high horizontal resolution versions. This model, together with surface data sets of albedo, roughness, surface resistance and grid area canopy fraction, forms Phase I of a longer term plan to improve surface and boundary-layer representation in these GCMs. Phase II will consider in more detail the problems associated with surface boundary-layer mixing, heterogeneity and boundary-layer clouds.

Together with the basic description of the soil-canopy model, we have provided numerous examples of the model performance, by comparing 1D simulations with more detailed mesoscale model simulations and observations.

The surface data sets (based on Dorman and Sellers, 1989) provide the means of specifying several parameters for up to twelve surface types distributed realistically in space. The soil-canopy model allows realistic fluxes to be calculated as a function of time of day, for each of these 12 surface types.

One final comment should be made regarding the coding of the 1D S/A scheme for use in a GCM. The simulations described in this technical paper are based on a 1D S/A scheme model coded explicitly for a small time step $\Delta t \leq 1min$. For application in a GCM, where $\Delta t \approx 30min$, an implicit scheme is required which must be formulated carefully to minimise numerical errors. The problem is particularly critical for the calculation of surface temperature from eqs.44 and 48. Details are beyond the scope of the present text.

References

- Bhumralkar, C.M., 1975: Numerical Experiments on the Computation of Ground Surface Temperature in Atmospheric General Circulation Models. J.Appl.Meteor., 14, 1246-1258.

- Blackadar, A.K., 1979: High-Resolution Models of the Planetary Boundary Layer. In Advances in Environmental Science and Engineering, Vol.1, Ed. by J.R. Pfafflin and E.N. Zeigler, Gordon and Breach, New York, 50-85.

- Carson, D.J., 1982: Current Parameterizations of Land-Surface Processes in Atmospheric General Circulation Models. In Land Surface Processes in Atmospheric General Circulation Models. Ed. by P.S. Eagleson, C.U.P., London, pp.67-108.

- Clapp, R.B. and G.M. Hornberger, 1978: Empirical Equations for Some Soil Hydraulic Properties. Water Resour. Res., 14, 601-604.

- Clarke, R.H., Dyer, A.J., Brook, R.R., Reid, D.G. and A.J. Troup, 1971: The Wangara Experiment: Boundary-Layer Data. Tech. Paper No.19, Div. Meteor. Physics, CSIRO, Australia. 21pp.

- Cosby, B.J., Hornberger, G.M., Clapp, R.B. and T.R. Ginn, 1984: A Statistical Exploration of the Relationships of Soil Moisture Characteristics to the Physical Properties of Soils. Water Resour. Res., 20, 682-690.

- Deacon, E.L., 1953: Vertical Profiles of Mean Wind in the Surface Layers of the Atmosphere. Geophys.Mem.No.91, 64pp.

- Deardorff, J.W., 1977: A Parameterization of Ground-Surface Moisture Content for Use in Atmospheric Prediction Models. J.Appl. Meteor., 16, 1182-1185.

- Deardorff, J.W., 1978: Efficient Prediction of Ground Surface Temperature and Moisture, with Inclusion of a Layer of Vegetation. J.Geophys. Res., 83 , 1889-1903.

- Dickinson, R.E., 1984: Modeling Evapotranspiration for Three Dimensional Global Climate Models. Climate Processes and Climate Sensitivity. Geophys.Monogr., 29, 58-72.

- Dickinson, R.E., Henderson-Sellers, A., Kennedy, P.J. and M.F. Wilson, 1986: Biosphere-Atmosphere Transfer Scheme (BATS) for the NCAR Community Climate Model. NCAR Technical Note NCAR/TN-275+STR, 69pp.

- Dorman, J.L. and P.J. Sellers, 1989: A Global Climatology of Albedo, Roughness Length and Stomatal Resistance for Atmospheric General Circulation Models as Represented by the Simple Biosphere Model (SiB). J.Appl.Meteor., 28, 833-855.

- Gates, D.M., 1980: Biophysical Ecology. Springer-Verlag, New York, 611pp.

- Garratt, J.R., 1977: Review of Drag Coefficients Over Oceans and Continents. Mon. Wea. Rev., 105, 915-929.

- Garratt, J.R., 1978: Transfer Characteristics for a Heterogeneous Surface of Large Aerodynamic Roughness. Quart.J.Roy.Met.Soc., 104, 491-502.

- Garratt, J.R., 1980: Surface Influence upon Vertical profiles in the Atmospheric Near-Surface Layer. Quart. J. Roy. Met. Soc., 106, 803-819.

- Garratt, J.R., Pittock, A.B. and K.,Walsh, 1990: Response of the A.B.L. and Soil Layer to a high Altitude, Dense Aerosol Cover. J.Appl. Meteor., 29, 35-52.

- Garratt, J.R., 1991: The Atmospheric Boundary Layer. Cambridge University Press, In Press.

- Garratt, J.R., 1992a: On the Sensitivity of Climate Simulations to Land-Surface and Atmospheric Boundary Layer Treatments in GCMs - A Review. J. Climate, In Press.

- Garratt, J.R., 1992b: Extreme Maximum Land-Surface Temperatures. J.Appl.Meteor., In Press.

- Henderson-Sellers, A. and M.F. Wilson, 1983: Surface Albedo Data for Climatic Modelling. Rev.Geoph. Space Phys., 21, 1743-1778.

- Hicks, B.B., 1973: Eddy Fluxes Over a Vineyard. Agric.Meteor., 12, 203-215.

- Hunt, B.G. and H.B. Gordon, 1989: Diurnally Varying Regional Climatic Simulations. Inter.J.Climatol., 9, 331-356.

- Idso, S.B., Aase, J.K. and R.D. Jackson, 1975: Net Radiation - Soil Heat Flux Relations as Influenced by Soil Water Content Variations. Bound. Layer Meteor., 9, 113-122.

- Izumi, Y., 1971: Kansas 1968 Field Program Data Report. Air Force Cambridge Res.Lab., Bedford, Mass., AFCRL-72-0041, Environ.Res. Papers, No.379, 79 pp.

- Jarvis, P.G., James, G.B. and J.J. Landsberg, 1976: Coniferous Forest. In Vegetation and the Atmosphere. Vol.2, Ed. by J.L. Monteith, Academic Press, New York, 171-240.

- Kriebel, K.T., 1979: Albedo of Vegetated Surfaces: Its Variability with Differing Irradiances. Remote Sens.Environ., 8, 283-290.

- Laval, K., 1988: Land Surface Processes. In Physically-Based Modelling and Simulation of Climate and Climatic Change - Part 1, Ed. by M.E. Schlesinger, Kluwer Acad.Pub., 285-306.

- Louis, J.F., 1979: A Parametric Model of Vertical Eddy Fluxes in the Atmosphere. Bound. Layer Meteor., 17, 187-202.

- Mahrt, L. and H. Pan, 1984: A Two-Layer Model of Soil Hydrology. Bound. Layer Meteor., 29, 1-20.

- Manabe, S., 1969: Climate and the Ocean Circulation. I The Atmospheric Circulation and the Hydrology of the Earth's Surface. Mon. Wea. Rev., 97, 739-774.

- Matthews, E., 1985: Atlas of Archived Vegetation, Land-Use and Seasonal Albedo Data Sets. NASA Tech.Memo.86199.

- McCumber, M.C. and R.A. Pielke, 1981: Simulation of the Effects of Surface Fluxes of Heat and Moisture in a Mesoscale Numerical Model 1. Soil Layer. J.Geophys.Res., 86, 9929-9938.

- Noilhan, J. and S. Planton, 1989: A Simple Parameterization of Land Surface rocesses for Meteorological Models. Mon.Wea.Rev., 117, 536-549.

- Oguntoyinbo, J.S., 1970: Reflection Coefficient of Natural Vegetation, Crops and Urban Surfaces in Nigeria. Quart.J.Roy.Meteor.Soc., 96, 430-441.

- Perrier, A., 1982: Land-Surface Processes: Vegetation. In Land Surface Processes in Atmospheric General Circulation Models. Ed. by P.S. Eagleson, C.U.P., London, pp.395-448.

- Pielke, R.A., 1984: Mesoscale Meteorological Modelling. Academic Press, New York, 612pp.

- Pinker, R.T., Thompson, O.E. and T.F. Eck, 1980: The Albedo of a Tropical Evergreen Forest. Quart.J.Roy.Meteor.Soc., 106, 551-558.

- Priestley, C.H.B. and R.J. Taylor, 1972: On the Assessment of Surface Heat Flux and Evaporation using Large-Scale Parameters. Mon.Wea. Rev., 100, 81-92.

- Russell, G., 1980: Crop Evaporation, Surface Resistance and Soil Water Status. Agric. Meteor., 21, 213-226.

- Rutter, A.J., 1975: The Hydrological Cycle in Vegetation. In Vegetation and the Atmosphere. Vol.1, Ed. by J.L. Monteith, Academic Press, New York, 111-154.

- Sato, N., Sellers, P.J., Randall, D.A., Schneider, E.K., Shukla, J., Kinter, J.L. III, Hou, Y.-T. and E. Albertazzi, 1989: Effects of Implementing the Simple Biosphere Model in a General Circulation Model. J.Atmos.Sci., 46, 2757-2782.

- Sellers, P.J., Mintz, Y., Sud, Y.C. and A. Dalcher, 1986: A Simple Biosphere Model (SiB) for Use Within General Circulation Models. J.Atmos.Sci., 43, 505-531.

- Shuttleworth, W.J. et al., 1984a: Observations of Radiation Exchange Above and Below Amazonian Forest. Quart.J.Roy.Met.Soc., 110, 1163-1169.

- Shuttleworth, W.J. et al., 1984b: Eddy Correlation of Energy Partition for Amazonian Forest. Quart.J.Roy.Met.Soc., 110, 1143-1162.

- Shuttleworth, W.J. and J.S. Wallace, 1985: Evaporation from Sparse Crops - An Energy Combination Theory. Quart.J.Roy.Met.Soc., 111, 839-855.

- Shuttleworth, W.J., 1989: Micrometeorology of Temperate and Tropical Forest. Phil.Trans.R.Soc. London, B324, 299-334.

- Stewart, J.B., 1971: The Albedo of a Pine Forest. Quart.J.Roy.Met. Soc., 97, 561-564.

- Tapper, N., 1988: Surface Energy Balance Studies in Australia's Tropics. Aust.Meteor.Mag., 36, 61-68.

- Toya, T. and N. Yasuda, 1988: Parameterization of Evaporation from a Non-saturated Bare Surface for Application in Numerical Prediction Models. Meteor. Soc. of Japan, Vol. 66, 729-739.

- Verma, S.B., Baldocchi, D.D., Anderson, D.E., Matt, D.R. and R.J. Clement, 1986: Eddy Fluxes of CO_2, Water Vapour, and Sensible Heat over a Deciduous Forest. Bound. Layer Meteor., 36, 71-91.

- Wilson, M.F. and A. Henderson-Sellers, 1985: A Global Archive of Land Cover and Soil Data Sets for Use in General Circulation Climate Models. J.Climatol., 5, 119-143.